RUNX2 Isoform II Protects Cancer Cells from Ferroptosis and Apoptosis by Promoting PRDX2 Expression in Oral Squamous Cell Carcinoma

Junjun Huang, [1] *Rong Jia,* [#, 1, 2] *Jihua Guo,* [#, 1, 3]

[1] State Key Laboratory of Oral & Maxillofacial Reconstruction and Regeneration, Key Laboratory of Oral Biomedicine Ministry of Education, Hubei Key Laboratory of Stomatology, School & Hospital of Stomatology, Wuhan University, Wuhan, 430079, China

[2] RNA Institute, Wuhan University, Wuhan, 430072, China

[3] Department of Endodontics, School & Hospital of Stomatology, Wuhan University, Wuhan, 430079, China

[#] Corresponding authors. jiarong@whu.edu.cn; jihuaguo@whu.edu.cn.

Abstract

Ferroptosis is a distinct iron-dependent programmed cell death and plays important roles in tumor suppression. However, the regulatory mechanisms of ferroptosis need further exploration. RUNT-related transcription factor 2 (RUNX2), a transcription factor, is essential for osteogenesis. RUNX2 has two types of transcripts produced by two alternative promoters. In the present study, we surprisingly find that RUNX2 isoform II is a novel ferroptosis and apoptosis suppressor. RUNX2 isoform II can bind to the promoter of peroxiredoxin-2 (*PRDX2*), a ferroptosis inhibitor, and activate its expression. Knockdown of RUNX2 isoform II suppresses cell proliferation *in vitro* and tumorigenesis *in vivo* in oral squamous cell carcinoma (OSCC). Interestingly, homeobox A10 (HOXA10), an upstream positive regulator of RUNX2 isoform II, is required for the inhibition of ferroptosis and apoptosis through the RUNX2 isoform II/PRDX2 pathway. Consistently, RUNX2 isoform II is overexpressed in OSCC, and associated with OSCC progression and poor prognosis. Collectively, OSCC cancer cells can up-regulate RUNX2 isoform II to inhibit ferroptosis and apoptosis, and facilitate tumorigenesis through the novel HOXA10/RUNX2 isoform II/PRDX2 pathway.

Research organism: Human, Mouse, Oral Squamous Cell Carcinoma

1. Introduction

Ferroptosis, a form of non-apoptotic programmed cell death, is an iron-dependent death and is characterized by the accumulation of lipid peroxidation and the production of reactive oxygen species (ROS) (Dixon et al., 2012). Ferroptosis has sparked great interest as targeting ferroptosis might provide new therapeutic opportunities in treating cancers. Emerging evidence indicates that ferroptosis may function as a potent tumor suppressor in the progression of head and neck squamous cell carcinoma (HNSCC) (Li, Jin, Zhang, Ma, & Yang, 2022; T. Lu et al., 2022), including oral squamous cell carcinoma (OSCC) (Sun et al., 2022; J. Yang, Cao, Luan, & Huang, 2021). Furthermore, triggering ferroptosis can overcome OSCC-acquired drug resistance such as cisplatin-induced resistance (Han, Li, & Wu, 2022). Therefore, the induction of ferroptosis is an attractive strategy for OSCC therapy. Multiple extrinsic or intrinsic pathways regulate the ferroptotic process (Tang & Kroemer, 2020). The extrinsic pathways are initiated by the inhibition of cell membrane transporters such as the cystine/glutamate transporter system xc^- or by the activation of the iron transporters transferrin (TF) and lactotransferrin (LTF). The intrinsic pathway is activated by the blockade of intracellular antioxidant enzymes like glutathione peroxidase 4 (GPX4). Although the principal regulatory mechanisms of ferroptosis have been explored in the past few years, other potential molecular mechanisms remain to be uncovered.

The RUNT-related transcription factor 2 (RUNX2), a member of the RUNT-related transcription factor family, is critical for osteogenesis (Bruderer, Richards, Alini, & Stoddart, 2014), and has been extensively studied in the development of bone and tooth (Wen et al., 2020; Ziros, Basdra, & Papavassiliou, 2008). Previous studies revealed that RUNX2 promotes cancer metastasis and invasion in a variety of cancers, including breast cancer (C. H. Chang et al., 2014), thyroid cancer (Sancisi et al., 2012), colorectal cancer (Ji et al., 2019), prostate cancer (Akech et al., 2010), lung cancer (Herreno et al., 2019) and HNSCC (W. M. Chang et al., 2016). However, the potential roles of RUNX2 in other aspects of tumorigenesis remain largely unclear. *RUNX2* gene is composed of two promoters that in turn generate two types of isoforms, isoform II derived from promoter 1 (P1) and isoform I from promoter 2 (P2). These isoforms contain distinct N-terminal sequences. Whether these isoforms play distinct roles in tumorigenesis remains unknown.

OSCC is one of the most common malignant cancers in the world, especially in areas with low Human Development Index (Sung et al., 2021). The treatment of OSCC has progressed over time from surgery alone to comprehensive series of therapies including radiation, chemotherapy and immunotherapy (Chi, Day, & Neville, 2015; Kang, Kiess, & Chung, 2015). Despite a lot of advances in treatment modalities, the five-year overall survival rate is around 50-60% (Jawert et al., 2021). Therefore, it is still challenging to improve the therapy of OSCC.

In this study, to have a well-defined understanding of the relationship between RUNX2 isoform II and ferroptosis, we examined the effects of isoform II-knockdown or -overexpression on total ROS levels and lipid peroxidation, apoptosis, and the effects of isoform II-knockdown on mitochondrial morphology in OSCC cells. And mechanically, peroxiredoxin-2 (PRDX2), a ferroptosis suppressor, was identified to be a target gene of RUNX2 isoform II. Meanwhile, we analyzed the effect of RUNX2 isoform II overexpression or knockdown on OSCC cell ferroptosis or apoptosis, cell proliferation and tumor growth.

2. Results

RUNX2 isoform II is overexpressed and associated with poor prognosis in OSCC

Given that the expression levels as well as the functions of RUNX2 isoforms (isoform I and II) produced by two alternative promoters (Figure 1A) in tumors are unclear, we explored their expression and roles in OSCC in this study. The expression levels of total RUNX2 were slightly higher in TCGA OSCC tissues than those in normal controls, but there was no statistically significant difference (Figure 1B). However, isoform I and II were significantly differently expressed in OSCC. The expression levels of isoform II (indicated by PSI, percent-splice-in, the usage of exon 1.1 in total RUNX2 transcripts) in OSCC patients were 1.46-fold significantly higher than those in normal controls (Figure 1C). In contrast, the expression levels of isoform I were lower than those in normal controls (Figure 1D). Moreover, patients with clinical stage I, II, and III showed lower levels of isoform II compared with those with stage IV (Figure 1E). Patients with higher isoform II showed significantly shorter overall survival (Figure 1F), whereas patients with higher isoform I showed longer overall survival (Figure 1-figure supplement 1). These evidences suggested that isoform II was highly expressed in OSCC tissues and positively correlated with the progression of OSCC.

Consistently, the expression levels of isoform II were also significantly upregulated in breast invasive carcinoma (BRCA) (Figure 1-figure supplement 2A), colon adenocarcinoma (COAD) (Figure 1-figure supplement 2B), prostate adenocarcinoma (PRAD) (Figure 1-figure supplement 2C), and stomach adenocarcinoma (STAD) (Figure 1-figure supplement 2D) patients of TCGA database, suggesting that isoform II might play extensive roles in multiple cancers.

To verify the results from TCGA, we analyzed the expression levels of RUNX2 isoforms in 11 OSCC tissues and adjacent normal controls by RT-PCR (Figure 1G). As expected, the ratios of isoform II vs I and the expression levels of isoform II were also significantly higher in these OSCC tissues than those in adjacent normal tissues (Figure 1H and I). These results suggested that RUNX2 isoform II may play important roles in OSCC.

RUNX2 isoform II is required for OSCC cell proliferation *in vitro* and tumorigenesis *in vivo*

Then, we explored the roles of RUNX2 isoform II in OSCC cells. Overexpression of FLAG tagged isoform II significantly promoted the proliferation of OSCC cells, CAL 27 and SCC-9 cell lines (Figure 2A and B, Figure 2-figure supplement 1A and B). Interestingly, isoform II overexpression showed enhanced cell proliferation compared with isoform I overexpression in OSCC cells (Figure 2A). Consistently, knockdown of isoform II significantly inhibited cell proliferation in both cell lines (Figure 2C and D), as well as colony formation (Figure 2E). We found that isoform II overexpression has no effect on OSCC cell migration or invasion, while isoform I overexpression could inhibit the cell migration or invasion (Figure 2- figure supplement 2A-C). Cells with isoform II-knockdown showed significantly higher apoptosis than those control cells (Figure 2F). However, the overexpression of isoform II or isoform I had no obvious effect on the cellular apoptosis of OSCC (Figure 2-figure supplement 3). Importantly, CAL 27 cells stably transfected with shRNAs against isoform II showed significantly reduced tumor growth and weight than those transfected with non-specific control shRNA in nude mice (Figure 2G-J, Figure 2-figure supplement 4A-D). These results suggested that RUNX2 isoform II is required for the proliferation and tumorigenicity of OSCC cells.

RUNX2 isoform II suppresses ferroptosis

Next, we explored how RUNX2 isoform II enhanced the proliferation of OSCC cells. Ferroptosis is an important form of programmed cell death and plays an important role in the suppression of tumors (Ouyang et al., 2022; Wei et al., 2021). We found that OSCC tissues had positive 4-hydroxynonenalince (4-HNE, a metabolite of lipid peroxidation) staining in variant levels, suggesting that ferroptosis might be present in OSCC tissues (Figure 3-figure supplement 1). Ferroptosis is characterized by the accumulation of lipid peroxidation and ROS. We found that isoform II-knockdown significantly enhanced total ROS production (Figure 3A) and lipid peroxidation accumulation (Figure 3B) in CAL 27 and SCC-9 cells. Consistently, isoform II overexpression suppressed ROS production (Figure 3C) and lipid peroxidation (Figure 3D) in these cells. In addition, we found that isoform II-knockdown induced shrunken mitochondria with vanished cristae with transmission electron microscopy (Figure 3E). This phenomenon along with the above results of ROS production and lipid peroxidation accumulation assays suggests that RUNX2 isoform II may suppress ferroptosis. We also found that isoform II-knockdown cells showed more elongated mitochondria than in control cells (Figure 3E and Figure 3-figure supplement 2A), which may be related to the suppression of FIS1 (Fission, Mitochondrial 1) expression by RUNX2 isoform II-knockdown (Figure 3-figure supplement 2B). And the elongated mitochondria may be caused by the deficiency of mitochondrial fission (Wang et al.,

2024). The oxygen consumption rates (OCR) were lower in isoform II-knockdown OSCC cells (Figure 3-figure supplement 3A and B). To further figure out whether isoform II could promote cell proliferation by inhibiting cell death, especially ferroptosis and apoptosis, we performed the rescue experiments with some inhibitors of cell death including ferrostatin-1 (Fer-1, a ferroptosis inhibitor), Z-VAD (an apoptosis inhibitor) and necrostatin-1 (Nec-1, a necroptosis inhibitor) upon isoform II-knockdown. As expected, Fer-1 treatment partially rescued the reduction of cell proliferation caused by isoform II-knockdown (Figure 3F and Figure 3-figure supplement 4A). We also found that Z-VAD and Nec-1 could partially rescue the reduction of cell proliferation caused by isoform II-knockdown (Figure 3G and Figure 3-figure supplement 4B) and Z-VAD also could partially decrease apoptosis induced by isoform II-knockdown (Figure 3-figure supplement 5), which suggested that both apoptosis and necroptosis also contribute to the retardation of cell proliferation cause by isoform II-knockdown. In addition, we found that the combination of Fer-1 and Z-VAD was more effective in rescuing cell proliferation than Fer-1 or Z-VAD alone (Figure 3- figure supplement 6). Fer-1 treatment reduced the increased levels of ROS production (Figure 3H) and lipid peroxidation (Figure 3I) caused by isoform II-knockdown. RSL3, a ferroptosis activator, could cause cell death in CAL 27 and SCC-9 cells (Figure 3-figure supplement 7A), and increase the production of cellular ROS (Figure 3-figure supplement 7B) and lipid peroxidation (Figure 3-figure supplement 7C). Isoform II overexpression could elevate the IC_{50} values of RSL3 (Figure 3-figure supplement 8A), in contrast, isoform II-knockdown decreased the IC_{50} values of RSL3 (Figure 3-figure supplement 8B). As expected, overexpression of isoform II could partially reduce the increased levels of ROS production (Figure 3J) and lipid peroxidation (Figure 3K) caused by RSL3. Consistently, tumors formed by CAL 27 cells with isoform II-knockdown showed a significantly increased staining of 4-HNE compared with the control (Figure 3L). In summary, these results suggested that RUNX2 isoform II can suppress ferroptosis in OSCC cells.

RUNX2 isoform II promotes the expression of PRDX2

To understand the regulatory mechanisms of how RUNX2 isoform II suppresses ferroptosis, we screened some ferroptosis-suppressive genes including several antioxidant enzymes in CAL 27 treated with isoform II siRNAs. Firstly, we found that RUNX2 isoform II-knockdown or overexpression could downregulate or upregulate the expression of GPX4 mRNA and protein, respectively (Figure 4-figure supplement 1A-D). In addition to the GPX4, we found that *PRDX2* is the most significantly down-regulated gene upon isoform II-knockdown in CAL 27 (Figure 4A). Furthermore, both mRNA and protein expression levels of PRDX2 were reduced in CAL 27 and SCC-9 cells with isoform II-knockdown (Figure 4B and C). Consistently, tumors formed by CAL 27 cells with isoform II-knockdown also showed a significantly reduced expression of PRDX2 compared with the control (Figure 4D). Isoform II

overexpression increased PRDX2 mRNA and protein expression (Figure 4E and F). Whereas, isoform I overexpression has no significant effect on PRDX2 expression (Figure 4E and F). In line with the inhibitory effect of isoform II-knockdown on tumor growth, CAL 27 cells stably transfected with anti-PRDX2 shRNAs showed notably reduced tumor growth and weight than those transfected with non-specific control shRNA in nude mice (Figure 4-figure supplement 2A-D). These results indicated that PRDX2 was a target of RUNX2 isoform II. One of the important characteristics of ferroptosis is the imbalance in iron homeostasis, and iron transporter transferrin receptor (TFRC) has an important role in maintaining iron homeostasis. We found that RUNX2 isoform II-knockdown in OSCC cells had no obvious effect on the expression of TFRC (Figure 4-figure supplement 3A and B). And the expression level and localization of TFRC did not change in the tumors formed by CAL 27 with or without isoform II-knockdown (Figure 4-figure supplement 3C). These results indicated that RUNX2 isoform II might not regulate the cellular transport of iron.

To explore the regulatory mechanisms of how RUNX2 isoform II promotes PRDX2 expression, we applied the JASPAR to predict possible binding sites of RUNX2 on the *PRDX2* promoter. We analyzed 0-2440 bp upstream regions of the *PRDX2* transcription start site and found 6 potential binding sites for RUNX2 on the *PRDX2* promoter (Figure 4G). Chromatin immunoprecipitation and quantitative PCR (ChIP-qPCR) assay showed that RUNX2 isoform II could specifically bind to the *PRDX2* promoter (Figure 4H and I) and the amplified region is the base represented by the red box (Figure 4G). These results suggested that isoform II could bind to the *PRDX2* promoter and transactivate PRDX2 expression.

To further verify whether PRDX2 mediated the effect of isoform II on ferroptosis, we stably overexpressed FLAG-tagged PRDX2 in CAL 27 cells. We found that overexpression of PRDX2 could partially reduce the elevated cellular ROS levels (Figure 4J) and lipid peroxidation levels (Figure 4K) induced by isoform II-knockdown in CAL 27 (Figure 4L and M). In addition, we found that PRDX2 overexpression could partially reduce the increased apoptosis caused by isoform II-knockdown (Figure 4-figure supplement 4). These data indicated that isoform II-knockdown promoted ferroptosis or apoptosis through inhibiting PRDX2 expression.

HOXA10 is required for RUNX2 isoform II expression and cell proliferation in OSCC

Next, we tried to understand the molecular mechanism of RUNX2 isoform II overexpression in OSCC cells. HOXA10 is an oncogenic transcription factor (L. M. Guo et al., 2018; Song et al., 2019). Mouse Hoxa10 has been reported to bind to Runx2 P1 promoter and then activate Runx2 isoform II expression in mouse cells (Hassan et al., 2007). Therefore, we speculated that RUNX2 isoform II overexpression in OSCC may be also caused by HOXA10. Indeed, HOXA10 knockdown significantly reduced isoform II expression in both CAL 27 and SCC-9

cells (Figure 5A), whereas isoform I expression was not significantly affected (Figure 5-figure supplement 1A). In line with the function of isoform II in OSCC cells, HOXA10 knockdown also significantly suppressed cell proliferation and colony formation (Figure 5B and C), and increased cellular apoptosis (Figure 5D). The expression levels of HOXA10 in TCGA OSCC patients were also significantly higher than those in normal controls (Figure 5-figure supplement 1B). Similarly, HOXA10 expression level of our clinical OSCC tissues is significantly higher than that of adjacent normal tissues (Figure 5-figure supplement 2A and B). Moreover, TCGA OSCC patients with higher expression levels of HOXA10 showed shorter overall survival (Figure 5-figure supplement 2C). Consistently, the expression levels of isoform II were positively correlated with HOXA10 expression levels in TCGA OSCC patients (Figure 5E). These results suggested that HOXA10 can promote RUNX2 isoform II expression.

HOXA10 inhibits ferroptosis and apoptosis through RUNX2 isoform II

Since RUNX2 isoform II was a ferroptosis and apoptosis suppressor, we speculated that HOXA10 could act as a ferroptosis and apoptosis inhibitor through upregulating the expression of isoform II. We found that the expression levels of PRDX2 mRNA and protein significantly decreased in parallel with the reduction in isoform II expression caused by HOXA10 knockdown (Figure 6A and B). In addition, HOXA10-knockdown could suppress the expression of GPX4 mRNA and protein (Figure 6-figure supplement 1A and B). Importantly, HOXA10 knockdown increased cellular ROS production (Figure 6C) and lipid peroxidation (Figure 6D) in CAL 27 and SCC-9 cells. Moreover, Fer-1, a ferroptosis inhibitor, could partially rescue the retarded cell proliferation caused by HOXA10 knockdown (Figure 6E and Figure 6-figure supplement 2A). We also found that Z-VAD (an apoptosis inhibitor) (Figure 6F and Figure 6-figure supplement 2B), Nec-1 (a necroptosis inhibitor) (Figure 6F and Figure 6-figure supplement 2B) could partially rescue the reduction of cell proliferation, and Z-VAD could also partially rescue the elevated apoptosis induced by HOXA10 knockdown (Figure 6-figure supplement 3). The combination of Fer-1 and Z-VAD was more effective in rescuing cell proliferation than Fer-1 or Z-VAD alone (Figure 6-figure supplement 4). Fer-1 could partially decrease the cellular ROS levels (Figure 6G) and lipid peroxidation (Figure 6H) caused by HOXA10-knockdown. Stable overexpression of isoform II could partially rescue the retarded cell proliferation caused by HOXA10 knockdown (Figure 7A). The increased cellular apoptosis (Figure 7B), ROS production levels (Figure 7C) and lipid peroxidation levels (Figure 7D) caused by HOXA10 knockdown were also reduced in these OSCC cells (Figure 7-figure supplement 1A and B). Collectively, these results demonstrated that HOXA10 is required for OSCC cancer cell proliferation by increasing RUNX2 isoform II expression, and decreasing ferroptosis and apoptosis.

In addition, isoform II overexpression could partially rescue the expression of PRDX2 in both mRNA and protein levels in OSCC cells treated with anti-HOXA10 siRNA (Figure 7E and F). In addition, we also found that PRDX2 overexpression could partially decrease the cellular ROS levels (Figure 7G) and lipid peroxidation levels (Figure 7H) induced by HOXA10 knockdown (Figure 7-figure supplement 1C and D). PRDX2 overexpression also could rescue the increased cellular apoptosis caused by HOXA10 knockdown (Figure 7-figure supplement 2). These data showed that HOXA10 knockdown promoted the ferroptosis and apoptosis in OSCC cells, partially through PRDX2, a downstream target of isoform II.

3. Discussion

Ferroptosis is a new form of programmed cell death and is caused by massive lipid peroxidation-mediated membrane damage (Stockwell et al., 2017). Emerging evidence has proved that ferroptosis contributes to the suppression of tumor progression. p53 could suppress the transcription of amino acid antiporter solute carrier family 7 member 11 (SLCA711) to sensitize cells to ferroptosis, which may contribute to the anti-tumor role of p53 (Jiang et al., 2015). Tumor inhibition by BRCA1-associated protein 1 (BAP1) could be achieved in part by inhibiting SLC7A11 and thereby promoting ferroptosis (Zhang et al., 2018). In HNSCC, Inhibition of xCT could suppress cell proliferation by inducing ferroptosis (M. Li et al., 2022). In addition, caveolin-1 (CAV-1) also could promote HNSCC progression through inhibiting ferroptosis (T. Lu et al., 2022). Therefore, enhancing ferroptosis could be an attractive strategy for OSCC treatment. In this study, we discovered a novel ferroptosis suppressor, RUNX2 isoform II, in OSCC. Isoform II overexpression or knockdown inhibited or promoted OSCC cell ferroptosis by decreasing or increasing total ROS levels and lipid peroxidation, respectively. One of the characteristics of ferroptosis is elevated cellular ROS levels, thus ferroptosis can be modulated by antioxidants (Tang, Chen, Kang, & Kroemer, 2021). For example, peroxiredoxin-6 (PRDX6) is a negative regulator of ferroptosis (B. Lu et al., 2019). In this study, we identified a new target gene for isoform II, the ferroptosis suppressor PRDX2. PRDX2 is a typical 2-Cys antioxidant enzyme belonging to the peroxiredoxin family and plays an important role in scavenging ROS levels (De Franceschi et al., 2011) through consuming H_2O_2 (W. Lu et al., 2014). We found that isoform II overexpression or knockdown promoted or suppressed PRDX2 expression, respectively. We found that isoform II knockdown also could induce apoptosis in OSCC cells, and PRDX2 overexpression could also reduce the elevated apotpsis induced by isoform II-knockdown. Moreover, isoform II could specifically bind to the promoter of *PRDX2* and then transactivate the PRDX2 expression, thereby inhibiting OSCC cell ferroptosis.

In this study, we also found that RUNX2 isoform II was overexpressed in OSCC tissues and was associated with tumor progression and poor prognosis. In the past years, it has been reported that RUNX2 was overexpressed in tumors (Akech et al.,

2010; Z. Guo et al., 2021; Hong et al., 2020). Chang et al. demonstrated that RUNX2 was overexpressed in HNSCC samples (W. M. Chang et al., 2017) and could serve as a poor prognostic marker in HNSCC (W. M. Chang et al., 2016). However, only a few articles have addressed the expression levels of isoforms. For example, isoform I is the major variant in papillary thyroid carcinomas (Sancisi et al., 2012), and isoform II is highly expressed in non-small cell lung cancer (Herreno et al., 2019). However, the expression levels of isoforms in OSCC are unknown. Surprisingly, our results showed that there was no statistically significant difference in expression levels of total RUNX2 between OSCC patients and normal controls from the TCGA database. Interestingly, we discovered that the expression levels of isoform I were lower in TCGA OSCC patients than in normal tissues, while the expression levels of isoform II were overexpressed in TCGA OSCC tissues. Furthermore, we proved with clinical samples that the relative expression levels of isoform II were higher in OSCC tissues than those in normal tissues.

Next, we uncovered the underlying mechanisms of RUNX2 isoform II to improve proliferation in OSCC cell lines. In the past, it has been reported that overexpression or knockdown of total RUNX2 in HNSCC cell lines could promote or inhibit cell proliferation, respectively (W. M. Chang et al., 2017). In this study, we found that isoform II overexpression or specific isoform II-knockdown could promote or suppress OSCC cell proliferation, respectively. In addition, we also demonstrated that isoform II was required for *in vivo* OSCC tumorigenesis.

Subsequently, we discovered that HOXA10 knockdown inhibited the expression of RUNX2 isoform II and led to ferroptosis and apoptosis. HOXA10, a transcription factor, plays an important role in tumor progression (J. Li et al., 2022; Song et al., 2019). HOXA10 was reported to transactivate Runx2 P1 promoter (Hassan et al., 2007). Similarly, we found that the relative expression levels of HOXA10 were positively associated with the expression levels of isoform II in OSCC patients from TCGA and HOXA10 knockdown led to the downregulation of isoform II in OSCC cells. It has been demonstrated that HOXA10 knockdown suppressed cell proliferation and enhanced apoptosis in Fadu cells (L. M. Guo et al., 2018). We found that HOXA10 knockdown inhibited cell proliferation and promoted cellular apoptosis in CAL 27 and SCC-9 through suppressing RUNX2 isoform II expression. Interestingly, we discovered that HOXA10 knockdown induced ferroptosis through suppressing RUNX2 isoform II and PRDX2 expression, which suggested a new regulatory pathway of anti-ferroptosis.

In conclusion, we identified RUNX2 isoform II as a novel ferroptosis and apoptosis inhibitor in OSCC cells by transactivating PRDX2 expression. RUNX2 isoform II plays oncogenic roles in OSCC. Moreover, we also found that HOXA10 is an upstream regulator of RUNX2 isoform II and is required for suppressing ferroptosis and apoptosis through RUNX2 isoform II and PRDX2. Our results suggest a new regulatory mechanism of ferroptosis through HOXA10/RUNX2 isoform II/PRDX2

pathway (Figure 7I) and may provide the novel diagnostic markers and therapeutic targets for OSCC.

4. Materials and Methods

Human tissues

The human OSCC tissues and adjacent normal tissues were collected from the Hospital of Stomatology in Wuhan University. The research was approved by the Ethics Committee at the Hospital of Stomatology in Wuhan University (2023-B03) and the study methodologies conformed with standards of the Declaration of Helsinki. Informed consents were obtained from all participants. Eleven patients diagnosed with OSCC were used in this study. All histologic diagnoses were performed by the Department of Pathology of the Hospital of Stomatology. The characteristics of the eleven OSCC patients were summarized in Table S1.

Nude mice xenograft tumor formation assay

BALB/c nude mice (female, 5-6 weeks) were purchased from Beijing Vital River Laboratory Animal Technology Co., Ltd (Vital River, Beijing, China). Animal experiments comply with the ARRIVE guidelines and were performed with the approval of the institutional Animal Ethics Committee, Hospital of Stomatology, Wuhan University (S07922110B).

CAL 27 cells stably transfected with short hairpin RNAs (shRNAs) against RUNX2 isoform II (shisoform II-1, shisoform II-2), with shRNA against PRDX2 (shPRDX2-1, shPRDX2-2) or nonspecific shRNA (shNC) through lentivirus were injected subcutaneously into both sides of the dorsum of nude mice (3.5×10^5 cells per injection side, 6 mice per group). Tumor sizes were monitored every 2 or 3 days. Tumor volume was calculated as Length x Width^2 x 0.52. Tumor weights were acquired after the mice were sacrificed on day 21.

Cell culture

CAL 27 and SCC-9 cells were obtained as previously reported (S. Yang, Jia, & Bian, 2018). HEK 293T cells were obtained from Procell Life Science (Procell, Wuhan, China). CAL 27 and HEK 293T were maintained in Dulbecco's modified Eagle's medium (DMEM) (Hyclone, Marlborough, MA, USA) supplemented with 10% fetal bovine serum (FBS) (Gibco, Carlsbad, CA, USA) and 1% antibiotic-antimycotic (Gibco). SCC-9 was cultured in DMEM/F12 medium (Hyclone) with 10% FBS, 1% antibiotic-antimycotic and 400 ng/mL hydrocortisone (Sangon Biotech, Shanghai, China). All cells were incubated at 37°C in 5% CO_2 humidified air.

Plasmids and transfection

The gene fragments of human RUNX2 isoform II and isoform I were amplified from CAL 27 cDNA by using the primers 5' ATGGCATCAAACAGCCTCTTC 3' and 5' ATATGGTCGCCAAACAGATTCATC 3', 5' ATGCGTATTCCCGTAGATCCG 3' and 5' ATATGGTCGCCAAACAGATTCATC 3', respectively. And then the PCR products were cloned into p3XFLAG-CMV-14 at BamHI and EcoRV sites. The respective FLAG-fusion fragments were then cloned into pLVX-IRES-puro vector at EcoRI and SpeI sites to obtain the recombinant expression plasmids isoform II or isoform I.

The gene fragment of human PRDX2 was amplified from CAL 27 cDNA by using the primers 5' ATCGTCCGTGCGTCTAGCCTT 3' and 5' ATTGTGTTTGGAGAAATATTCCTTGCT 3'. And the PCR product was re-amplified by 5' TTCCGGAATTCGCCACCATGGCCTCCGGTAA 3' and 5' TTCGCGCGGCCGCCTACTTGTCATCGTCATCCTTGTAGTCGATGTCATGATC TTTATAATCACCGTCATGGTCTTTGTAGTCTTTTGCCGCAGCTTC 3' to obtain PRDX2-FLAG fusing fragment, and then was cloned into pLVX-IRES-puro vector at EcoRI and NotI to obtain the recombinant expression plasmid PRDX2.

HEK-293T cells were co-transfected with 2 μg lentiviral backbone plasmids (isoform II, isoform I, PRDX2 or control vector, pLVX-IRES-puro) and the packaging plasmids psPAX2 and pMD2.G at a ratio 4:3:1 in the presence of Lipofectamine 2000 (Invitrogen, Carlsbad, CA, USA). The supernatants containing lentiviral particles were collected 48 hours after transfection. OSCC cell lines were then transfected with lentiviral supernatants in the presence of polybrene (Santa Cruz, Dallas, TX, USA).

TCGA datasets

We downloaded the data of total RUNX2 and HOXA10 expression levels, and the clinical data in patients with OSCC of TCGA HNSCC dataset from the online program TSVdb (http://www.tsvdb.com). Then, we re-analyzed the expression levels of total RUNX2 and HOXA10 between OSCC patients and normal controls (309 OSCC cases and 32 normal cases). The percent-splice-in (PSI) value data representing the expression levels of exon 1.1 (isoform II) or exon 2.1 (isoform I) of OSCC (288 OSCC cases and 27 normal cases with PSI values) and other carcinomas were obtained from the online program TCGA SpliceSeq (https://bioinformatics.mdanderson.org/TCGA/SpliceSeq).

RNA extraction and reverse transcription polymerase chain reaction (RT-PCR)

Total RNA was purified using the AxyPrep multisource total RNA miniprep Kit (Axygen, Union City, CA, USA) according to the manufacturer's protocol. Total RNA was treated with DNase I (Thermo Fisher Scientific, Carlsbad, CA, USA) to remove genomic DNA contamination and then was reversely transcribed by using the Maxima

H Minus cDNA Synthesis Master Mix (Thermo Fisher Scientific) in accordance with the manufacturer's protocol. The cDNA was subject to PCR amplification using Green Taq Mix (Vazyme, Nanjing, China) with different primers. The primer sequences are listed in Table S2.

RNA interference and transfection

The short interfering RNAs (siRNAs) against human RUNX2 isoform II were synthesized by Sangon Biotech. The sequences are as follows: 5' GCUUCAUUCGCCUCACAAACA 3' (si-II-1) and 5' GGUUAAUCUCCGCAGGUCACU 3' (si-II-2). The siRNAs, synthesized by GenePharma (Suzhou, China), were used to knock down human HOXA10 (siHOX-1 and siHOX-2). The sequences of siHOX-1 and siHOX-2 are 5' GAGUUUCUGUUCAAUAUGUACCUUA 3' and 5' CCGGGAGCUCACAGCCAACUUUAAU 3', respectively. Cells were transfected with 20 nM siRNAs in the presence of Lipofectamine 3000 (Invitrogen) according to the manufacturer's protocol. After 48 h, cells were transfected again.

The short hairpin RNAs (shRNAs) against RUNX2 isoform II (shisoform II-1, shisoform II-2) plasmids, against PRDX2 (shPRDX2-1, shPRDX2-2) plasmids and non-specific shRNA (shNC) plasmid were provided by Vector Builder Inc (Vector Builder, Guangzhou, China). The target sequences of shisoform II-1 and shisoform II-2 are GGTTAATCTCCGCAGGTCACT and GCTTCATTCGCCTCACAAACA. The target sequences of shPRDX2-1 and shPRDX2-2 are GCCTGGCAGTGACACGATTAA and CCTTCGCCAGATCACTGTTAA. The plasmids shisoform II or shNC were co-transfected with psPAX2 and pMD2.G into HEK 293T cells to produce supernatants containing lentiviruses. Then the supernatants containing lentiviral particles were collected 48 hours after transfection to transfect CAL 27 OSCC cell line in the presence of polybrene.

Immunohistochemistry (IHC)

The mouse tumor tissues or human OSCC tissues were fixed in 4% paraformaldehyde (Servicebio, Wuhan, China), and embedded in paraffin, then sectioned in 4 μm. The staining of PRDX2, TFRC or 4-HNE was detected by using a Dako EnVision FLEX kit (Dako, Glostrup, Denmark) according to the manufacturer's instructions. Briefly, the sections were subjected to antigen retrieval in Target Retrieval Solution (Dako). Endogenous peroxidase was blocked with Peroxidase-Blocking Reagent (Dako). Then, the sections were incubated with primary antibody (PRDX2, TFRC or 4-HNE) at 4°C overnight and followed by incubation with secondary antibody FLEX/HRP (Dako) at room temperature for 30 min. Staining was developed by diaminobenzidine (DAB) substrate (Dako). The stained sections were scanned by Pannoramic MIDI (3D HISRECH). The concentration of PRDX2

(Proteintech, Wuhan, China, #10545-2-AP), 4-HNE (Abcam, Cambridge, UK, ab48506) or TFRC (Abcam, ab214039) used in this study was 1:1000, 1:600 or 1:500, respectively.

Chromatin immunoprecipitation and quantitative PCR (ChIP & qPCR)

ChIP was performed in CAL 27 cells stably transfected by FLAG-tagged RUNX2 isoform II or vector (pLVX-IRES-puro) using ABclonal Sonication Chip Kit (ABclonal, Wuhan, China) according to the manufacturer's protocol. In brief, cells in 10-cm culture dishes were crosslinked with 1% formaldehyde and the reaction was terminated by glycine. Cells were lysed, and samples were then sonicated to disrupt the nuclear membrane. After centrifugation, the supernatants were collected which contained the chromatin. Chromatin solutions were, respectively, incubated with antibodies anti-FLAG (2 μg, Proteintech, #20543-1-AP) and anti-normal rabbit IgG (2 μg, ABclonal, #RM20712). And then, they were rotated at 4°C for 6 hours, followed by incubation with ChIP-grade protein A/G magnetic beads (ABclonal, #RM02915) at 4°C for 2 hours. After washing, the cross-links were reversed at 65°C overnight, and DNA was purified (ABclonal, #RK30100) and then used for ChIP-qPCR analysis. For the ChIP-qPCR experiments with a pair of primers for the *PRDX2* promoter region as follow: 5' TACAGGTGTGAGCCAGCCACCAT 3' (forward primer) and 5' TGGCGGGCACCAAGGATGTTGT 3' (reverse primer).

Western blot

Cells were lysed with 2 x SDS sample buffer, and then the total cellular protein was denatured for 3 min at 95°C. Total cellular proteins were separated in 4-12% YoungPAGE Bis-Tris gels (GenScript, Nanjing, China) or 10% gels using One-Step PAGE Gel Fast Preparation Kit (Vazyme), transferred to nitrocellulose membrane (Pall Corporation, USA), followed by the block with 5% (w/v) non-fat milk (Servicebio) for 1 h. Then the membranes were incubated with mouse RUNX2 antibody (1:500, Santa Cruz, #sc-390351), rabbit FLAG antibody (1:2000, Proteintech, #20543-1-AP), rabbit PRDX2 antibody (1:2000, Proteintech, #10545-2-AP), GPX4 antibody (1:1000, ABclonal, #A11243) and mouse actin antibody (1:5000, Proteintech, #66009-1-lg).

Cell counting and colony formation assay

Cell counting was performed by the trypan blue exclusion method using 0.4% trypan blue solution (Biosharp, Hefei, China). One thousand CAL 27 or SCC-9 cells were seeded into 6-well plates and cultured in complete medium for 11 days at 37°C. Then, cells were fixed with 4% paraformaldehyde and stained with crystal violet (Servicebio). The number of colonies (at least 50 cells/colony) was counted.

Wound healing assay

For wound healing, cells with stable expression of isoform II, isoform I or vector were plated in six-well plates and grown to 90-100% concentration. The artificial wounds were created with pipette tips, and then cells were cultured in serum-free medium after washing with PBS. The migrating cells in the wound front were imaged at different times. Wound healing status was analyzed by ImageJ.

Transwell migration and invasion assays

The migration and invasion assays were performed by using Transwell chamber (Corning, USA). For migration assay, 5×10^4 SCC-9 with stable expression of isoform II, isoform I or vector per well were seeded into the upper chambers with serum-free medium. The lower chambers were contained the complete medium. For invasion assay, the 8 μm pore transwell filters were pre-coated with Matrigel (Corning, USA), and the subsequent steps were similar to the migration assay. After the cells migrated or invaded for certain time, they were fixed with 4% paraformaldehyde, stained by 0.1% crystal violet. The transwell filters were imaged and analyzed by ImageJ.

Apoptosis assay

Cell apoptosis was analyzed using the Annexin V-FITC/PI apoptosis assay kit (KeyGEN BioTECH, Nanjing, China, #KGA108). Briefly, the cells were collected in 200 μL binding buffer with 2 μL of Annexin V-FITC and 2 μL PI, and incubated for 20 min under dark conditions. Cellular apoptosis was evaluated using flow cytometry.

ROS detection

The total cellular ROS was detected using a ROS assay kit DCFH-DA (Beyotime, Shanghai, China, #S0033S). DCFH-DA was diluted to a final concentration of 10 μM. Then, OSCC cell lines were collected and suspended in diluted DCFH-DA in the dark at 37°C for 25 min and washed 3 times with PBS. The samples were analyzed using flow cytometry.

Transmission electron microscopy (TEM)

Cells cultured in a 6-well plate were collected and fixed with a solution containing 2.5% glutaraldehyde (Servicebio) for 2 hours in the dark at room temperature. Then the ultrathin sections were made by Servicebio and visualized by using the JEM-1011 transmission electron microscope (Hitachi, Japan). The length of mitochondria was analyzed by Nano Measurer, and the average mitochondrial length of each group was summarized.

Detection of lipid peroxidation

OSCC cells were collected and suspended in PBS containing 5 μM C11-BODIPY 581/591 (Thermo Fisher Scientific, #D3861) in the dark at 37°C for 30 min and washed 3 times with PBS, and the samples were analyzed using flow cytometry through the FITC channel.

Oxygen consumption rate (OCR) assay

To assess the impact of isoform II knockdown on mitochondrial respiration in OSCC cells, Seahorse Bioscience XFe24 (Agilent Seahorse XFe24 Analyzer) was used according to the manufacturer's instructions. The mitochondrial respiration was analyzed by using the Mito-stress Test Kit. Briefly, $3x10^4$ SCC-9 cells were seeded in 24-well plates and incubated overnight. Cells were washed and incubated in Seahorse detection buffer at 37°C in no CO_2 for 1h. The OCR was tested using the compounds of oligomycin (1 μM), FCCP (1 μM) and rotenone and antimycin A (Rot/AA, 1 μM).

Half-maximal inhibitory concentration (IC_{50}) of RSL3

Cells were seeded in 24-well plates ($2x10^4$ cells/well) overnight, then treated with RSL3 at different concentration (0.125, 0.25, 0.5, 1, 2, 4, 8, 16, 32 μM). The cells were counted on the next day. The IC_{50} values of RSL3 were analyzed by GraphPad Prism.

Statistical analysis

The comparison of the mean values between three groups or more was performed using the one-way ANOVA test in the GraphPad Prism software. The Mann-Whitney test was used to compare the mean differences of RUNX2 exon 1.1 (isoform II) or exon 2.1 (isoform I) in COAD and PRAD from TCGA, the mean difference of isoform II expression levels (isoform II/GAPDH) or HOXA10 expression levels in our clinical samples, the weight and volume of mouse tumors (shisoform II), the H score of 4-HNE staining of mouse tumors, and the expression levels of HOXA10 in TCGA OSCC patients. All remaining two-group comparisons of means were analyzed by Student's *t*-test. The Kruskal-Wallis test was used to compare the tumor growth in nude mice between non-specific control and shPRDX2. Survival analysis was performed with a log-rank test and survival curve was produced using the Kaplan-Meier method in the GraphPad Prism software. The correlation of RUNX2 exon 1.1 (isoform II) was calculated with the Spearman rank method. The quantification of RT-PCR was realized using imageJ software. $P < 0.05$ was considered statistically significant.

Competing interests

The authors declare no conflict of interest.

Acknowledgement

This study was supported by the National Natural Science Foundation of China grant numbers 81970933 and 82170966.

Author Contributions

Conceptualization: J.G. and R.J. Data Curation: J.H. Formal analysis: J.H. Funding acquisition: J.G. and R.J. Investigation: J.H. Methodology: J.H. J.G. and R.J. Project administration: J.G. and R.J. Resources: J.G. and R.J. Supervision: J.G. and R.J. Validation: J.H. J.G. and R.J. Visualization: J.H. Writing-original draft preparation: J.H. Writing-review and editing: J.G. and R.J.

Data and Materials Availability Statement

All data needed to evaluate the conclusions in the paper are present in this article or the supplementary materials. All materials may be made available to the scientific community upon request.

Ethics

Human research was approved by the Ethics Committee at the Hospital of Stomatology in Wuhan University (2023-B03) and the study methodologies conformed with standards of the Declaration of Helsinki. Informed consents were obtained from all participants.

Animal experiments comply with the ARRIVE guidelines and were performed with the approval of the institutional Animal Ethics Committee, Hospital of Stomatology, Wuhan University (S07922110B).

References

Akech, J., Wixted, J. J., Bedard, K., van der Deen, M., Hussain, S., Guise, T. A., . . . Lian, J. B. (2010). Runx2 association with progression of prostate cancer in patients: mechanisms mediating bone osteolysis and osteoblastic metastatic lesions. *Oncogene, 29*(6), 811-821. doi:10.1038/onc.2009.389

Bruderer, M., Richards, R. G., Alini, M., & Stoddart, M. J. (2014). Role and regulation of RUNX2 in osteogenesis. *Eur Cell Mater, 28*, 269-286. doi:10.22203/ecm.v028a19

Chang, C. H., Fan, T. C., Yu, J. C., Liao, G. S., Lin, Y. C., Shih, A. C., . . . Yu, A. L. (2014). The prognostic significance of RUNX2 and miR-10a/10b and their inter-relationship in breast cancer. *J Transl Med, 12*, 257. doi:10.1186/s12967-014-0257-3

Chang, W. M., Lin, Y. F., Su, C. Y., Peng, H. Y., Chang, Y. C., Hsiao, J. R., . . . Shiah, S. G. (2017). Parathyroid Hormone-Like Hormone is a Poor Prognosis Marker of Head and Neck Cancer and Promotes Cell Growth via RUNX2 Regulation. *Sci Rep, 7*, 41131. doi:10.1038/srep41131

Chang, W. M., Lin, Y. F., Su, C. Y., Peng, H. Y., Chang, Y. C., Lai, T. C., . . . Shiah, S. G. (2016). Dysregulation of RUNX2/Activin-A Axis upon miR-376c Downregulation Promotes Lymph Node Metastasis in Head and Neck Squamous Cell Carcinoma. *Cancer Res, 76*(24), 7140-7150. doi:10.1158/0008-5472.CAN-16-1188

Chi, A. C., Day, T. A., & Neville, B. W. (2015). Oral cavity and oropharyngeal squamous cell carcinoma--an update. *CA Cancer J Clin, 65*(5), 401-421. doi:10.3322/caac.21293

De Franceschi, L., Bertoldi, M., De Falco, L., Santos Franco, S., Ronzoni, L., Turrini, F., . . . Iolascon, A. (2011). Oxidative stress modulates heme synthesis and induces peroxiredoxin-2 as a novel cytoprotective response in β-thalassemic erythropoiesis. *Haematologica, 96*(11), 1595-1604. doi:10.3324/haematol.2011.043612

Dixon, S. J., Lemberg, K. M., Lamprecht, M. R., Skouta, R., Zaitsev, E. M., Gleason, C. E., . . . Stockwell, B. R. (2012). Ferroptosis: an iron-dependent form of nonapoptotic cell death. *Cell, 149*(5), 1060-1072. doi:10.1016/j.cell.2012.03.042

Guo, L. M., Ding, G. F., Xu, W., Ge, H., Jiang, Y., Chen, X. J., & Lu, Y. (2018). MiR-135a-5p represses proliferation of HNSCC by targeting HOXA10. *Cancer Biol Ther, 19*(11), 973-983. doi:10.1080/15384047.2018.1450112

Guo, Z., Zhou, K., Wang, Q., Huang, Y., Ji, J., Peng, Y., . . . Yang, Z. (2021). The transcription factor RUNX2 fuels YAP1 signaling and gastric cancer tumorigenesis. *Cancer Sci, 112*(9), 3533-3544. doi:10.1111/cas.15045

Han, L., Li, L., & Wu, G. (2022). Induction of ferroptosis by carnosic acid-mediated inactivation of Nrf2/HO-1 potentiates cisplatin responsiveness in OSCC cells. *Mol Cell Probes, 64*, 101821. doi:10.1016/j.mcp.2022.101821

Hassan, M. Q., Tare, R., Lee, S. H., Mandeville, M., Weiner, B., Montecino, M., . . . Lian, J. B. (2007). HOXA10 controls osteoblastogenesis by directly activating bone regulatory and phenotypic genes. *Mol Cell Biol, 27*(9), 3337-3352. doi:10.1128/mcb.01544-06

Herreno, A. M., Ramirez, A. C., Chaparro, V. P., Fernandez, M. J., Canas, A., Morantes, C. F., . . . Rojas, A. P. (2019). Role of RUNX2 transcription factor in epithelial mesenchymal transition in non-small cell lung cancer lung cancer: Epigenetic control of the RUNX2 P1 promoter. *Tumour Biol, 41*(5), 1010428319851014. doi:10.1177/1010428319851014

Hong, Z., Fang, Z., Lei, J., Shi, G., Zhang, Y., He, Z., . . . Zhong, S. (2020). The significance of Runx2 mediating alcohol-induced Brf1 expression and RNA Pol III gene transcription. *Chem Biol Interact, 323*, 109057. doi:10.1016/j.cbi.2020.109057

Jawert, F., Nyman, J., Olsson, E., Adok, C., Helmersson, M., & Ohman, J. (2021). Regular clinical follow-up of oral potentially malignant disorders results in improved survival for patients who develop oral cancer. *Oral Oncol, 121*, 105469. doi:10.1016/j.oraloncology.2021.105469

Ji, Q., Cai, G., Liu, X., Zhang, Y., Wang, Y., Zhou, L., . . . Li, Q. (2019). MALAT1 regulates the transcriptional and translational levels of proto-oncogene RUNX2 in colorectal cancer metastasis. *Cell Death Dis, 10*(6), 378. doi:10.1038/s41419-019-1598-x

Jiang, L., Kon, N., Li, T., Wang, S. J., Su, T., Hibshoosh, H., . . . Gu, W. (2015). Ferroptosis as a p53-mediated activity during tumour suppression. *Nature, 520*(7545), 57-62. doi:10.1038/nature14344

Kang, H., Kiess, A., & Chung, C. H. (2015). Emerging biomarkers in head and neck cancer in the era of genomics. *Nat Rev Clin Oncol, 12*(1), 11-26. doi:10.1038/nrclinonc.2014.192

Li, J., Chang, J., Wang, J., Xu, D., Yang, M., Jiang, Y., . . . Sun, Y. (2022). HOXA10 promote pancreatic cancer progression via directly activating canonical NF-kappaB signaling pathway. *Carcinogenesis, 43*(8), 787-796. doi:10.1093/carcin/bgac042

Li, M., Jin, S., Zhang, Z., Ma, H., & Yang, X. (2022). Interleukin-6 facilitates tumor progression by inducing ferroptosis resistance in head and neck squamous cell carcinoma. *Cancer Lett, 527*, 28-40. doi:10.1016/j.canlet.2021.12.011

Lu, B., Chen, X. B., Hong, Y. C., Zhu, H., He, Q. J., Yang, B., . . . Cao, J. (2019). Identification of PRDX6 as a regulator of ferroptosis. *Acta Pharmacol Sin, 40*(10), 1334-1342. doi:10.1038/s41401-019-0233-9

Lu, T., Zhang, Z., Pan, X., Zhang, J., Wang, X., Wang, M., . . . Chen, W. (2022). Caveolin-1 promotes cancer progression via inhibiting ferroptosis in head and neck squamous cell carcinoma. *J Oral Pathol Med, 51*(1), 52-62. doi:10.1111/jop.13267

Lu, W., Fu, Z., Wang, H., Feng, J., Wei, J., & Guo, J. (2014). Peroxiredoxin 2 knockdown by RNA interference inhibits the growth of colorectal cancer cells by downregulating Wnt/β-catenin signaling. *Cancer Lett, 343*(2), 190-199. doi:10.1016/j.canlet.2013.10.002

Ouyang, S., Li, H., Lou, L., Huang, Q., Zhang, Z., Mo, J., . . . Zhang, X. (2022). Inhibition of STAT3-ferroptosis negative regulatory axis suppresses tumor growth and alleviates chemoresistance in gastric cancer. *Redox Biol, 52*, 102317. doi:10.1016/j.redox.2022.102317

Sancisi, V., Borettini, G., Maramotti, S., Ragazzi, M., Tamagnini, I., Nicoli, D., . . . Ciarrocchi, A. (2012). Runx2 isoform I controls a panel of proinvasive genes driving aggressiveness of papillary thyroid carcinomas. *J Clin Endocrinol Metab, 97*(10), E2006-2015. doi:10.1210/jc.2012-1903

Song, C., Han, Y., Luo, H., Qin, Z., Chen, Z., Liu, Y., . . . Zhou, C. (2019). HOXA10 induces BCL2 expression, inhibits apoptosis, and promotes cell proliferation in gastric cancer. *Cancer Med, 8*(12), 5651-5661. doi:10.1002/cam4.2440

Stockwell, B. R., Friedmann Angeli, J. P., Bayir, H., Bush, A. I., Conrad, M., Dixon, S. J., . . . Zhang, D. D. (2017). Ferroptosis: A Regulated Cell Death Nexus Linking Metabolism, Redox Biology, and Disease. *Cell, 171*(2), 273-285. doi:10.1016/j.cell.2017.09.021

Sun, K., Ren, W., Li, S., Zheng, J., Huang, Y., Zhi, K., & Gao, L. (2022). MiR-34c-3p upregulates erastin-induced ferroptosis to inhibit proliferation in oral squamous cell carcinomas by targeting SLC7A11. *Pathol Res Pract, 231*, 153778. doi:10.1016/j.prp.2022.153778

Sung, H., Ferlay, J., Siegel, R. L., Laversanne, M., Soerjomataram, I., Jemal, A., & Bray, F. (2021). Global Cancer Statistics 2020: GLOBOCAN Estimates of Incidence and Mortality Worldwide for 36 Cancers in 185 Countries. *CA Cancer J Clin, 71*(3), 209-249. doi:10.3322/caac.21660

Tang, D., Chen, X., Kang, R., & Kroemer, G. (2021). Ferroptosis: molecular mechanisms and health implications. *Cell Res, 31*(2), 107-125. doi:10.1038/s41422-020-00441-1

Tang, D., & Kroemer, G. (2020). Ferroptosis. *Curr Biol, 30*(21), R1292-r1297. doi:10.1016/j.cub.2020.09.068

Wang, Z., Tang, S., Cai, L., Wang, Q., Pan, D., Dong, Y., . . . Chen, Q. (2024). DRP1 inhibition-mediated mitochondrial elongation abolishes cancer stemness, enhances glutaminolysis, and drives ferroptosis in oral squamous cell carcinoma. *Br J Cancer, 130*(11), 1744-1757. doi:10.1038/s41416-024-02670-2

Wei, R., Zhao, Y., Wang, J., Yang, X., Li, S., Wang, Y., . . . Ding, X. (2021). Tagitinin C induces ferroptosis through PERK-Nrf2-HO-1 signaling pathway in colorectal cancer cells. *Int J Biol Sci, 17*(11), 2703-2717. doi:10.7150/ijbs.59404

Wen, Q., Jing, J., Han, X., Feng, J., Yuan, Y., Ma, Y., . . . Chai, Y. (2020). Runx2 Regulates Mouse Tooth Root Development Via Activation of WNT Inhibitor NOTUM. *J Bone Miner Res, 35*(11), 2252-2264. doi:10.1002/jbmr.4120

Yang, J., Cao, X. H., Luan, K. F., & Huang, Y. D. (2021). Circular RNA FNDC3B Protects Oral Squamous Cell Carcinoma Cells From Ferroptosis and

Contributes to the Malignant Progression by Regulating miR-520d-5p/SLC7A11 Axis. *Front Oncol, 11*, 672724. doi:10.3389/fonc.2021.672724

Yang, S., Jia, R., & Bian, Z. (2018). SRSF5 functions as a novel oncogenic splicing factor and is upregulated by oncogene SRSF3 in oral squamous cell carcinoma. *Biochim Biophys Acta Mol Cell Res, 1865*(9), 1161-1172. doi:10.1016/j.bbamcr.2018.05.017

Zhang, Y., Shi, J., Liu, X., Feng, L., Gong, Z., Koppula, P., . . . Gan, B. (2018). BAP1 links metabolic regulation of ferroptosis to tumour suppression. *Nat Cell Biol, 20*(10), 1181-1192. doi:10.1038/s41556-018-0178-0

Ziros, P. G., Basdra, E. K., & Papavassiliou, A. G. (2008). Runx2: of bone and stretch. *Int J Biochem Cell Biol, 40*(9), 1659-1663. doi:10.1016/j.biocel.2007.05.024

Figure legends

Figure 1. Human RUNX2 isoform II is overexpressed and associated with poor prognosis in OSCC. (A) Schematic diagram of the isoforms and alternative promoters of the human *RUNX2* gene. Boxes and lines represent exons or introns in the pre-mRNA, respectively. P1 and P2 represent promoters. Isoform II is transcribed from P1, while isoform I is transcribed from P2. Exon 5 and 7 are alternative exons. (B-D) The expression levels of total RUNX2 and isoforms in TCGA OSCC patients. (B) The normalized expression levels of total RUNX2, obtained from an online program, TSVdb, in normal (32 cases) or OSCC tissues (309 cases). (C, D) The PSI (percent-splice-in) values of exon 1.1 (isoform II) (C) and exon 2.1 (isoform I) (D) (total 288 cases with PSI values of exon 1.1 and exon 2.1) in normal (27 cases) and OSCC tissues (288 cases) were obtained from an online program, TCGA SpliceSeq. The PSI values represent the relative expression levels of individual isoform. (E) Comparison of exon 1.1 (isoform II) PSI between patients in stage I, II and III (132 cases) and those in stage IV (156 cases) of OSCC TCGA patients. (F) OSCC TCGA patients (total 286 cases with survival data) with low expression (254 cases) or high expression (32 cases) of exon 1.1 (isoform II) in OSCC. Low exon 1.1 (isoform II) PSI was defined as less than mean + 1.427SD (standard deviation). (G) The representative RT-PCR results of isoform II and isoform I in our OSCC or normal samples. GAPDH served as a loading control. (H-I) The scatter dot plot summarized the ratio of isoform II versus isoform I (isoform II/isoform I) (H) or the relative expression levels of isoform II (isoform II/GAPDH) (I) in our clinical OSCC (11 cases) and normal samples (11 cases). * $P < 0.05$, ** $P < 0.01$.

Figure 2. RUNX2 isoform II is required for the proliferation *in vitro* and tumorigenesis *in vivo*. (A) CAL 27 or SCC-9 cells were stably transfected by isoform II-expression, isoform I-expression or vector control lentivirus. CAL 27 cells were seeded into 24-well plates at day 0 and counted on day 1, 2 and 3. SCC-9 cells were seeded into 24-well plates at day 0 and counted on day 2 and 4. Data are means ± SD, n = 3. (B) Overexpression of RUNX2 isoform II or isoform I was confirmed by Western blot. Actin served as a loading control. (C) Proliferation curves of CAL 27 and SCC-9 cells treated with anti-isoform II siRNAs (si-II-1 or si-II-2) or negative control siRNA (NC). Data are means ± SD, n = 3. (D) Knockdown efficiency of isoform II was analyzed by RT-PCR. GAPDH served as a loading control. (E) Effects of isoform II-knockdown on the clonogenic ability in CAL 27 and SCC-9. The histograms on the right summarized the numbers of colonies (at least 50 cells/colony). Data are means ± SD, n = 3. (F) CAL 27 and SCC-9 cells were treated with si-II-1, si-II-2 or NC siRNA. The cellular apoptosis was analyzed by flow cytometry. The histograms on the right summarized the cellular apoptosis. Data are means ± SD, n = 4 for CAL 27, n = 3 for SCC-9. (G-I) CAL 27 cells with stable isoform II shRNA (shisoform II-1) or nonspecific shRNA (shNC) were injected into both sides of the dorsum of BALB/c nude mice. (G, H) Tumors were dissected out and weighed on day 21. (I) Tumor volumes were measured on different days. (J) Knockdown efficiency of isoform II was analyzed by RT-PCR. 18S rRNA served as a loading control. * $P < 0.05$, ** $P < 0.01$, *** $P < 0.001$.

Figure 3. RUNX2 isoform II suppresses ferroptosis. (A, B) CAL 27 and SCC-9 cells were treated with anti-isoform II siRNAs (si-II-1 and si-II-2) or negative control siRNA (NC). (A) The levels of total ROS were detected with DCFH-DA using flow cytometry. The histograms below summarized the levels of mean fluorescent intensity (MFI). Data are means ± SD, n = 4. (B) The lipid peroxidation of cells was analyzed with C11 BODIPY 581/591 reagent using flow cytometry. The histograms below summarized the levels of MFI. Data are means ± SD, n = 4 for CAL 27, n = 3 for SCC-9. (C, D) CAL 27 or SCC-9 cells were stably transfected by isoform II-expression or vector control lentivirus. The levels of ROS (C) or lipid peroxidation (D) were detected by flow cytometry. The histograms below summarized the levels of MFI. Data are means ± SD, n = 4. (E) Transmission electron microscopy images of CAL 27 cells transfected with si-II-1, si-II-2 or NC. RSL3 (a ferroptosis activator) served as a positive control. Scale bar: 1 μm (F) CAL 27 cells transfected with anti-isoform II siRNAs were also treated with ferrostatin-1 (Fer-1, 10 μM), a ferroptosis inhibitor. Negative control siRNA and DMSO were used as controls. Cells were divided into six groups: NC+DMSO, si-II-1+DMSO, si-II-2+DMSO, NC+Fer-1, si-II-1+Fer-1 and si-II-2+Fer-1. To display clear diagrams, the proliferation curves of si-II-1-treated cells or si-II-2-treated cells were shown separately. Data are means ± SD, n = 3. (G) CAL 27 cells transfected with anti-isoform II siRNAs were also treated with Z-VAD (20 μM, an apoptosis inhibitor) or necrostatin-1 (Nec-1, 20 μM, a necroptosis inhibitor). Negative

control siRNA and DMSO were used as controls. Cells were divided into nine groups: NC+DMSO, si-II-1+DMSO, si-II-2+DMSO, NC+Z-VAD, si-II-1+Z-VAD, si-II-2+Z-VAD, NC+Nec-1, si-II-1+Nec-1, si-II-2+Nec-1. To display clear diagrams, the proliferation curves of si-II-1-transfected cells or si-II-2-transfected cells were shown separately. Data are means ± SD, n = 3. (H, I) The total ROS levels (H) or lipid peroxidation (I) of cells simultaneously transfected with anti-isoform II siRNAs or NC and treated with Fer-1 or DMSO were detected with DCFH-DA (H) or BODIPY 581/591 reagent (I) by flow cytometry. The histogram on the right summarized the levels of MFI. Data are means ± SD, n = 3. (J, K) The total ROS levels (J) or lipid peroxidation (K) of isoform II-overexpressed cells treated with RSL3 (2 μM, a ferroptosis activator) or DMSO were detected with DCFH-DA (J) or BODIPY 581/591 reagent (K) by flow cytometry. The histogram on the right summarized the levels of MFI. Data are means ± SD, n = 4 for J, n = 5 for K. (L) Representative images of immunohistochemical staining of 4-HNE in tumors with or without isoform II-knockdown (shisoform II *vs* shNC) in Figure 2G. The histogram below summarized the H score of 4-HNE staining in tumors. * $P < 0.05$, ** $P < 0.01$, *** $P < 0.001$.

Figure 4. RUNX2 isoform II promotes the expression of PRDX2. (A) Screening analysis of the expression of enzymatic antioxidant genes upon isoform II-knockdown (si-II-1 and si-II-2) in CAL 27 cells *via* RT-PCR. (B, C) Effects of RUNX2 isoform II-knockdown on PRDX2 expression levels were analyzed by RT-PCR (B) or Western blot (C) in CAL 27 or SCC-9. 18S rRNA (B) or actin (C) served as loading controls. Data are means ± SD, n = 3. (D) Representative images of immunohistochemical staining of PRDX2 in tumors with or without isoform II-knockdown (shisoform II *vs* shNC) in Figure 2G. The histogram below summarized the expression levels of PRDX2 in tumors. (E, F) Effects of RUNX2 isoform II or isoform I overexpression on PRDX2 expression levels were analyzed by RT-PCR (E) or Western blot (F) in CAL 27 or SCC-9. 18S rRNA (E) or actin (F) served as loading controls. Data are means ± SD, n = 6 or 3 for CAL 27, n = 3 for SCC-9. (G) RUNX2 binding motifs on *PRDX2* promoter were obtained from JASPAR. (H) Chromatin immunoprecipitation and quantitative PCR (ChIP-qPCR) assay was performed in CAL 27 with or without FLAG-tagged RUNX2 isoform II overexpression (isoform II vs vector) by using anti-FLAG or control IgG antibody. Data are means ± SD, n = 3. (I) The immunoprecipitated protein levels of FLAG-tagged RUNX2 isoform II in the ChIP assays were determined by Western blot. (J-M) CAL 27 cells were co-transfected with PRDX2-expression, empty control lentivirus, and anti-isoform II siRNA (si-II), negative control siRNA (NC). Transfected cells were divided into four groups: Vector+NC, Vector+si-II, PRDX2+NC and PRDX2+si-II. (J, K) The total ROS levels (J) or lipid peroxidation (K) of transfected cells were detected with DCFH-DA (J) or BODIPY 581/591 reagent (K) by flow cytometry. The histograms below summarized the levels of MFI. Data are means ± SD, n = 3. (L) Overexpression of PRDX2 was confirmed by

Western blot. Actin served as a loading control. (M) Knockdown efficiency of isoform II was analyzed by RT-PCR. 18S rRNA served as a loading control. * $P < 0.05$, ** $P < 0.01$, *** $P < 0.001$.

Figure 5. HOXA10 is required for RUNX2 isoform II expression and cell proliferation in OSCC. (A) Effects of HOXA10 knockdown (siHOX-1 and siHOX-2) on isoform II expression levels were analyzed by RT-PCR in CAL 27 or SCC-9. 18S rRNA served as a loading control. Data are means ± SD, n = 3. (B-D) CAL 27 or SCC-9 cells were treated with siHOX-1, siHOX-2 or NC siRNA. (B) Proliferation curves of CAL 27 or SCC-9 cells treated with HOXA10 siRNAs or NC siRNA. Data are means ± SD, n = 3. (C) Effects of HOXA10 knockdown on the clonogenic ability in CAL 27 and SCC-9. The histograms on the right summarized the numbers of colonies (at least 50 cells/colony). Data are means ± SD, n = 3. (D) The cellular apoptosis was analyzed by flow cytometry. The histograms on the right summarized the cellular apoptosis. Data are means ± SD, n = 4 for CAL 27, n = 3 for SCC-9. (E) The expression of HOXA10 in TCGA OSCC patients (288 cases) is positively correlated with RUNX2 exon 1.1 (isoform II) PSI (Spearman's rank correlation coefficient, r=0.21, $P < 0.001$). * $P < 0.05$, ** $P < 0.01$, *** $P < 0.001$.

Figure 6. HOXA10 promotes the expression of PRDX2 and inhibits ferroptosis in OSCC. (A, B) Effects of HOXA10 knockdown (siHOX-1 and siHOX-2) on PRDX2 expression levels were analyzed by RT-PCR (A) or Western blot (B) in CAL 27 or SCC-9. 18S rRNA (A) or actin (B) served as loading controls. Data are means ± SD, n = 4 or 3 for CAL 27, n = 3 for SCC-9. (C, D) Effects of HOXA10 knockdown on ROS levels (C) or lipid peroxidation (D) were detected with DCFH-DA (C) or BODIPY 581/591 reagent (D) by flow cytometry in CAL 27 or SCC-9. The histograms below summarized the levels of MFI. Data are means ± SD, n = 4 for CAL 27, n = 3 or 4 for SCC-9. (E) CAL 27 cells transfected with anti-HOXA10 siRNAs were also treated with Fer-1 (10 μM), a ferroptosis inhibitor. Negative control siRNA and DMSO were used as controls. Cells were divided into six groups: NC+DMSO, siHOX-1+DMSO, siHOX-2+DMSO, NC+Fer-1, siHOX-1+Fer-1 and siHOX-2+Fer-1. To display clear diagrams, the proliferation curves of siHOX-1-treated cells or siHOX-2-treated cells were shown separately. Data are means ± SD, n = 3. (F) CAL 27 cells transfected with anti-HOXA10 siRNAs were also treated with Z-VAD (20 μM, an apoptosis inhibitor) or Nec-1 (20 μM, a necroptosis inhibitor). Negative control siRNA and DMSO were used as controls. Cells were divided into nine groups: NC+DMSO, siHOX-1+DMSO, siHOX-2+DMSO, NC+Z-VAD, siHOX-1+Z-VAD, siHOX-2+Z-VAD, NC+Nec-1, siHOX-1+Nec-1, siHOX-2+Nec-1. To display clear diagrams, the proliferation curves of siHOX-1-transfected cells or siHOX-2-transfected cells were shown separately. Data are means ± SD, n = 3. (G, H) The total ROS levels (H) or

lipid peroxidation (I) of cells simultaneously transfected with anti-HOXA10 siRNAs or NC and treated with Fer-1 or DMSO were detected with DCFH-DA (G) or BODIPY 581/591 reagent (H) by flow cytometry. The histogram on the right summarized the levels of MFI. Data are means ± SD, n = 3 for G, n=4 for H. * $P < 0.05$, ** $P < 0.01$, *** $P < 0.001$.

Figure 7. Ferroptosis and apoptosis induced by HOXA10-knockdown can be rescued by isoform II overexpression or PRDX2 overexpression. (A-F) CAL 27 cells were co-transfected with isoform II-expression lentivirus, empty control lentivirus, and HOXA10 siRNA (siHOX), negative control siRNA (NC). Transfected cells were divided into four groups: Vector+NC, Vector+siHOX, Isoform II+NC and Isoform II+siHOX. (A) Cell number was counted on day 2 and day 4. Data are means ± SD, n = 5. (B) The cellular apoptosis of transfected cells was analyzed by flow cytometry. The histogram on the right summarized the cell apoptosis. Data are means ± SD, n = 4. (C, D) The total ROS levels (C) or lipid peroxidation (D) of transfected cells were detected with DCFH-DA (C) or BODIPY 581/591 reagent (D) by flow cytometry. The histograms below summarized the levels of MFI. Data are means ± SD, n = 4 or 3. (E, F) Effect of HOXA10-knockdown in isoform II-overexpressed cells on PRDX2 expression levels was analyzed by RT-PCR (E) or Western blot (F). 18S rRNA (E) or actin (F) served as loading controls. Data are means ± SD, n = 3 or 4. (G, H) CAL 27 cells were co-transfected with PRDX2-expression lentivirus, empty control lentivirus, and siHOX, NC. Transfected cells were divided into four groups: Vector+NC, Vector+siHOX, PRDX2+NC and PRDX2+siHOX. The total ROS levels (G) or lipid peroxidation (H) of transfected cells were detected with DCFH-DA (G) or BODIPY 581/591 reagent (H) by flow cytometry. The histograms on the right summarized the levels of MFI. Data are means ± SD, n = 3. (I) The model of a new ferroptosis-related or apoptosis related pathway-HOXA10/RUNX2 isoform II/PRDX2 in this study. * $P < 0.05$, ** $P < 0.01$, *** $P < 0.001$.

Figure 1-figure supplement 1. Lower RUNX2 isoform I expression is associated with poor overall survival in OSCC patients. OSCC TCGA patients (total 286 cases with survival data) with low expression (32 cases) or high expression (254 cases) of exon 2.1 (isoform I) in OSCC. High exon 2.1 (isoform II) PSI was defined as more than mean - 1.427SD.

Figure 1-figure supplement 2. RUNX2 isoform II is also overexpressed in some other carcinomas. (A-D) The data valuing the expression levels of RUNX2 isoforms (indicated by percent-splice-in) were obtained from TCGA SpliceSeq. The expression levels of RUNX2 exon 1.1 (isoform II) and exon 2.1 (isoform I) were compared between normal (99 cases) and tumor tissues (1050 cases) in BRCA (A) patients, normal (39 cases) and tumor tissues (241 cases) in COAD (B) patients, normal (50

cases) and tumor tissues (320 cases) in PRAD (C) patients, normal (31 cases) and tumor tissues (397 cases) in STAD (D). * $P < 0.05$, *** $P < 0.001$.

Figure 2-figure supplement 1. RUNX2 isoform II overexpression promoted cell proliferation. CAL 27 were stably transfected by isoform II-expression, isoform I-expression or vector control lentivirus. (A) Cells were seeded in 24-well plates at day 0 and counted on day 1, 2 and 3. Data are means ± SD, n = 3. (B) Overexpression of RUNX2 isoform II or isoform I was confirmed by Western blot. * $P < 0.05$

Figure 2-figure supplement 2. RUNX2 isoform II has no effect on migration or invasion of OSCC cells. (A) Representative images of wound-healing in cells overexpressing isoform II, isoform I or vector (control). The histogram on the right summarized the relative migration rates. (B, C) Representative images of transwell migration (B) or invasion (C) in cells overexpressing isoform II, isoform I or control. The histograms on the right summarized the migrated cells (B) or invaded cells (C). Scale bar: 100 μm. Data are means ± SD, n = 3, ** $P < 0.01$.

Figure 2-figure supplement 3. Overexpression of RUNX2 isoform II or isoform I did not affect cellular apoptosis. The cellular apoptosis of CAL 27 or SCC-9 stably transfected by isoform II-expression, isoform I-expression or vector control lentivirus was analyzed by flow cytometry. The histograms on the right summarized the cellular apoptosis. Data are means ± SD, n = 3.

Figure 2-figure supplement 4. RUNX2 isoform II-knockdown inhibits the tumor growth. CAL 27 cells with another stable isoform II shRNA (shisoform II-2) or nonspecific shRNA (shNC) were injected into both sides of the dorsum of BALB/c nude mice. (A, B) Tumors were dissected out and weighed on day 34. (C) Tumor volumes were measured on different days. (D) Knockdown efficiency of isoform II was analyzed by RT-PCR. 18S rRNA served as a loading control. * $P < 0.05$, ** $P < 0.01$.

Figure 3-figure supplement 1. Ferroptosis may be present in OSCC tissues. The images of immunohistochemical staining of 4-HNE in OSCC tissues.

Figure 3-figure supplement 2. RUNX2 isoform II knockdown cells show more elongated mitochondria. (A) The histogram summarized the mitochondrial length. Data are means ± SD, n = 3. (B) Effects of isoform II-knockdown on the expression levels of FIS1 were analyzed by RT-PCR in CAL 27 or SCC-9 cells. 18S rRNA served as a loading control. Data are means ± SD, n = 4. * $P < 0.05$, ** $P < 0.01$, *** $P < 0.001$.

Figure 3-figure supplement 3. RUNX2 isoform II-knockdown inhibits oxygen consumption rate (OCR) in OSCC cells. (A) OCR detection in isoform II-knockdown of SCC-9. (B) Knockdown efficiency of RUNX2 isoform II (shisoform II-1 and shisoform II-2) was analyzed by RT-PCR. 18S rRNA served as a control.

Figure 3-figure supplement 4. Validation of RUNX2 isoform II-knockdown in Figure 3 (A) Knockdown efficiency of RUNX2 isoform II in ferrostatin-1 (Fer-1, a ferroptosis inhibitor) treated cells was analyzed by RT-PCR. 18S rRNA served as a control. (B) Knockdown efficiency of RUNX2 isoform II (si-II-1 and si-II-2) in Z-VAD, (an apoptosis inhibitor) or necrostatin-1 (Nec-1, a necroptosis inhibitor) treated cells was analyzed by RT-PCR. 18S rRNA served as a control.

Figure 3-figure supplement 5. The apoptosis inhibitor Z-VAD reduces the increased apoptosis rates caused by isoform II-knockdown. The cellular apoptosis of CAL 27 simultaneously transfected with siRNAs (anti-isoform II siRNAs or NC) and treated with Z-VAD or DMSO was detected by flow cytometry. The histogram on the right summarized the cellular apoptosis. Data are means ± SD, n = 3. ** $P < 0.01$, *** $P < 0.001$.

Figure 3-figure supplement 6. The combination of Fer-1 and Z-VAD patially rescues the deduced cell proliferation caused by isoform II knockdown. CAL 27 cells transfected with anti-isoform II siRNA (si-II) were also treated with DMSO, Fer-1 and Z-VAD. We analyzed the rescue efficiency of Fer-1 and Z-VAD alone or the combination of Fer-1 and Z-VAD in cell proliferation. The rescue efficiency of cells = (number of cells in inhibitor-treated and isoform II-knockdown group / number of cells in inhibitor-treated and NC group - number of cells in DMSO-treated and isoform II-knockdown group / number of cells in DMSO-treated and NC group)/1- (number of cells in DMSO-treated and isoform II-knockdown group / number of cells in DMSO-treated and NC group). Data are means ± SD, n = 3. *** $P < 0.001$.

Figure 3-figure supplement 7. OSCC cell lines are sensitive to RSL3 treatment. (A) The OSCC cells (CAL 27 or SCC-9) were seeded into 24-well plates at day 0. Then, the cells were treated with RSL3 (2 μM, a ferroptosis activator) or DMSO 24 hours after plating. The cells were counted at 12 and 24 hours after RLS3 treatment. Data are means ± SD, n = 4. (B, C) The total ROS levels (B) or lipid peroxidation (C) of cells treated with RSL3 or DMSO were detected with DCFH-DA (B) or BODIPY 581/591 reagent (C) by flow cytometry. The histogram below summarized the levels of MFI. Data are means ± SD, n = 4. ** $P < 0.01$, *** $P < 0.001$.

Figure 3-figure supplement 8. Half maximal inhibitory concentration (IC_{50}) of RSL3 was analyzed in isoform II-overexpression CAL 27 (A) or in isoform II-knockdown CAL 27 (B).

Figure 4-figure supplement 1. RUNX2 isoform II promotes the expression of GPX4 in OSCC cell lines. (A, B) Effects of isoform II-knockdown (si-II-1 and si-II-2) on the expression levels of GPX4 were analyzed by RT-PCR (A) or Western blot (B) in CAL 27 or SCC-9 cells. 18S rRNA (A) or actin (B) served as loading controls. Data are means ± SD, n = 3. (C, D) Effects of isoform II overexpression on the expression levels of GPX4 were analyzed by RT-PCR (C) or Western blot (D) in CAL 27 or SCC-9 cells. 18S rRNA (A) or actin (B) served as loading controls. Data are means ± SD, n = 3. * $P < 0.05$, ** $P < 0.01$, *** $P < 0.001$.

Figure 4-figure supplement 2. PRDX2-knockdown inhibits the tumor growth. CAL 27 cells with stable PRDX2 shRNAs (shPRDX2-1 and shPRDX2-2) or nonspecific shRNA (shNC) were injected into both sides of the dorsum of BALB/c nude mice. (A, B) Tumors were dissected out and weighed on day 25. (C) Tumor volumes were measured on different days. (D) Knockdown efficiency of PRDX2 was analyzed by Western blot. Actin served as a loading control. ** $P < 0.01$, *** $P < 0.001$.

Figure 4-figure supplement 3. RUNX2 isoform II has no effect on TFRC expression levels and localization in OSCC cells. (A, B) Effects of isoform II-knockdown (si-II-1 and si-II-2) on the expression levels of TFRC were analyzed by RT-PCR (A) or Western blot (B) in CAL 27 or SCC-9 cells. 18S rRNA (A) or actin (B) served as loading controls. (C) The representative images of immunohistochemical staining of TFRC in tumors with or without isoform II-knockdown (shisoform II *vs* shNC) in Figure 2G. The histogram on the right summarized the H score of TFRC staining. Data are means ± SD, n = 4.

Figure 4-figure supplement 4. PRDX2 overexpression rescue the apoptosis induced by isoform II knockdown. CAL 27 cells were co-transfected with PRDX2-expression lentivirus, empty control lentivirus, and isoform II siRNA (si-II), negative control siRNA (NC). Transfected cells were divided into four groups: Vector+NC, Vector+si-II, PRDX2+NC and PRDX2+si-II. The apoptosis of transfected cells were analyzed by flow cytometry. The histogram on the right summarized the apoptosis. Data are means ± SD, n = 4. *** $P < 0.001$.

Figure 5-figure supplement 1. HOXA10 does not affect the expression of isoform I. (A) Effects of HOXA10 knockdown (siHOX-1 and siHOX-2) on the isoform I expression in CAL 27 or SCC-9 were analyzed by RT-PCR. 18S rRNA served as a loading control. Data are means ± SD, n = 3. (B) The expression levels of HOXA10 in normal tissues (32 cases) or in OSCC tissues (309 cases) from TCGA. *** $P < 0.001$.

Figure 5-figure supplement 2. HOXA10 is overexpressed in OSCC and associated with poor overall survival. (A) The representative RT-PCR results of HOXA10 In our

OSCC or normal samples. GAPDH served as a loading control. (B) The scatter dot plot summarized the relative expression levels of HOXA10 (HOXA10/GAPDH) in our clinical OSCC (11 cases) and normal samples (11 cases). (C) OSCC TCGA patients (total 308 cases with survival data) with low expression (258 cases) or high expression (50 cases) of HOXA10 in OSCC. Low relative expression of HOX10 was defined as less than mean + 0.917SD.

Figure 6-figure supplement 1. HOXA10-knockdown inhibits PRDX2 expression. (A, B) Effects of HOXA10-knockdown on GPX4 expression levels were analyzed by RT-PCR (A) or Western blot (B) in CAL 27 or SCC-9. 18S rRNA (A) or actin (B) served as loading controls. Data are means ± SD, n = 3 for RT-PCR, n = 4 for Western blot. * $P < 0.05$, ** $P < 0.01$, *** $P < 0.001$.

Figure 6-figure supplement 2. Validation of HOXA10 knockdown in Figure 6. (A) Knockdown efficiency of HOXA10 in Fer-1 (a ferroptosis inhibitor) treated cells was analyzed by RT-PCR. 18S rRNA served as a control. (B) Knockdown efficiency of HOXA10 (siHOX-1 and siHOX-2) in Z-VAD, (an apoptosis inhibitor) or Nec-1(a necroptosis inhibitor) treated cells was analyzed by RT-PCR. 18S rRNA served as a control.

Figure 6-figure supplement 3. The increased apoptosis rates caused by HOXA10 knockdown could be rescued by apoptosis inhibitor Z-VAD. The cellular apoptosis of CAL 27 simultaneously transfected with anti-HOXA10 siRNAs or NC and treated with Z-VAD or DMSO were detected by flow cytometry. The histogram on the right summarized he cellular apoptosis. Data are means ± SD, n = 3. *** $P < 0.001$.

Figure 6-figure supplement 4. The combination of Fer-1 and Z-VAD partially rescues the deduced cell proliferation caused by HOXA10 knockdown. CAL 27 cells transfected with anti-isoform II siRNA (si-HOX) were also treated with DMSO, Fer-1 and Z-VAD. We analyzed the rescue efficiency of Fer-1 and Z-VAD alone or the combination of Fer-1 and Z-VAD in cell proliferation. The rescue efficiency of cells = (number of cells in inhibitor-treated and HOXA10-knockdown group / number of cells in inhibitor-treated and NC group - number of cells in DMSO-treated and HOXA10-knockdown group / number of cells in DMSO-treated and NC group)/1-(number of cells in DMSO-treated and HOXA10-knockdown group / number of cells in DMSO-treated and NC group). Data are means ± SD, n = 3. * $P < 0.05$. *** $P < 0.001$.

Figure 7-figure supplement 1. Validation of expression levels of HOXA10, RUNX2 isoform II and PRDX2 in Figure 7. (A) Knockdown efficiency of HOXA10 (anti-HOXA10 siRNA, siHOX) was analyzed by RT-PCR in isoform II-overexpressing CAL 27 cells. 18S rRNA served as a loading control. (B) Overexpression of RUNX2

isoform II was confirmed by Western blot. Actin served as a loading control. (C) Knockdown efficiency of HOXA10 was analyzed by RT-PCR in PRDX2-overexpressing CAL 27 cells. 18S rRNA served as a loading control. (D) Overexpression of PRDX2 was confirmed by Western blot. Actin served as a loading control.

Figure 7-figure supplement 2. PRDX2 overexpression rescue the apoptosis induced by isoform II knockdown. CAL 27 cells were co-transfected with PRDX2-expression lentivirus, empty control lentivirus, and isoform II siRNA (si-II), negative control siRNA (NC). Transfected cells were divided into four groups: Vector+NC, Vector+si-II, PRDX2+NC and PRDX2+si-II. The apoptosis of transfected cells were analyzed by flow cytometry. The histogram on the right summarized the apoptosis. Data are means ± SD, n = 4. *** $P < 0.001$.

Key Resources Table				
Reagent type (species) or resource	**Designation**	**Source or reference**	**Identifiers**	**Additional information**
strain, strain background (*Mus musculus)*	BALB/c nude mice	Vital River	Strain No.401	
cell line (*Homo sapiens*)	CAL 27 SCC-9	(S. Yang et al., 2018)		
cell line	HEK 293T	Procell	Cat# CL-0005	

(Human)				
transfected construct (Human)	RUNX2 isoform II shRNAs (shisoform II-1 and shisoform II-2)	Vector Builder	Cat# VB221206-1024udv; VB221206-1021ujk	Lentiviral construct to transfect and express the shRNA.
transfected construct (Human)	PRDX2 shRNAs (shPRDX-1 and shPRDX2-2)	Vector Builder	Cat# VB900064-6571eqq; VB900064-6578nnu	Lentiviral construct to transfect and express the shRNA.
transfected construct (Human)	Negative control shRNA (shNC)	Vector Builder	Cat# VB010000-009mxc	
transfected construct (Human)	siRNAs to isoform II (si-II-1/si-II-2)	Sangon Biotech		transfected construct (Human)
transfected construct (Human)	siRNAs to HOXA10 (siHOX-1/siHOX-2)	GenePharma		transfected construct (Human)

transfected construct (Human)	siRNA to negative control (siNC)	Sangon Biotech		
biological sample (Human)	Oral squamous cell carcinoma	Hospital of Stomatology, Wuhan University		The adjacent normal tissues were also acquired
antibody	anti-human RUNX2 (Mouse monoclonal)	Santa Cruz	Cat# SC-390351; RRID: AB_2892645	1:500
antibody	4-HNE	Abcam	Cat# ab48506; RRID: AB_867452	IHC: 1:600
antibody	TFRC	Abcam	Cat# ab214039; RRID: AB_2904534	WB: 1:2000 IHC: 1:500
antibody	anti-human FLAG (Rabbit polyclonal)	Proteintech	Cat# 20543-1-AP; RRID: AB_11232216	WB: 1:2000 ChIP：2 μg
antibody	anti-human/mouse PRDX2 (Rabbit polyclonal)	Proteintech	Cat# 10545-2-AP; RRID: AB_2168202	WB: 1:2000 IHC: 1:1000

antibody	anti-human actin (Mouse monoclonal)	Proteintech	Cat# 66009-1-lg; RRID: AB_2782959	1:5000
antibody	GPX4 Rabbit mAb	ABclonal	Cat# A11243 RRID: AB_2861533	1:1000
recombinant DNA reagent	RUNX2 isoform II (Plasmid)	This paper		FLAG-tagged isoform II
recombinant DNA reagent	RUNX2 isoform I (plasmid)	This paper		FLAG-tagged isoform I
recombinant DNA reagent	PRDX2 (plasmid)	This paper		FLAG-tagged PRDX2
commercial assay or kit	Total RNA Miniprep Kit	Axygen	Cat# AP-MN-MS-RNA-250	
commercial assay or kit	Green Taq Mix	Vazyme	Cat# P131-AA	

commercial assay or kit	Phanta® Super-Fidelity DNA Polymerase	Vazyme	Cat# P505-d1	
commercial assay or kit	Maxima™ H Minus cDNA Synthesis Master Mix	Thermo Fisher Scientific	Cat# M1682	
commercial assay or kit	ChamQ Universal SYBR qPCR Master Mix	Vazyme	Cat# Q711-02	
commercial assay or kit	Reactive Oxygen Species Assay Kit	Beyotime	Cat# S0033S	
commercial assay or kit	BODIPY™ 581/591 C11	Thermo Fisher Scientific	Cat# D3861	
commercial assay or kit	Annexin V-FITC/PI apoptosis assay kit	KeyGEN BioTECH	Cat# KGA108	
commercial assay or	Sonication ChIP Kit	Abclonal	Cat# RK20258	

kit				
commercial assay or kit	Protein A/G beads	Abclonal	Cat# RM02915	
commercial assay or kit	Protease Inhibitor Cocktail	Abclonal	Cat# RM02916	
commercial assay or kit	EnVision FLEX TARGET RETRIEVAL SOLUTION HIGH pH	Dako	REF# K8023	
commercial assay or kit	EnVision FLEX PEROXIDASE-BLOCOING REAGENT	Dako	REF# GV800	
commercial assay or kit	EnVision FLEX/HRP	Dako	REF# K8023	
commercial assay or kit	Liquid DAB+ Substrate Chromogen System	Dako	REF# K3468	

commercial assay or kit	XF Cell Mito Stress Test Kit	Agilent	Cat# 103015-100	
commercial assay or kit	Seahorse XF DMEM Assay Medium Pack	Agilent	Cat# 103680-100	
commercial assay or kit	Seahorse XFe24 FluxPak	Agilent	Cat# 102340wz-100	
chemical compound, drug	Ferrostatin-1	MCE	CAS# 347174-05-4	Dissolved in DMSO
chemical compound, drug	RSL3	MCE	CAS# 1219810-16-8	Dissolved in DMSO
chemical compound, drug	Z-VAD	Selleck	Cat# S7023	Dissolved in DMSO
chemical compound, drug	Necrostatin-1	Selleck	Cat# S8037	Dissolved in DMSO

chemical compound, drug	Polybrene	Santa Cruz	Cat# sc-134120	
chemical compound, drug	Lipofectamine ™ 2000	Thermo Fisher Scientific	Cat# 11668019	
chemical compound, drug	Lipofectamine ™ 3000	Thermo Fisher Scientific	Cat# L3000001	
software, algorithm	FlowJo	FlowJo	RRID: SCR_008520	
software, algorithm	GraphPad Prism	GraphPad Software	RRID: SCR_002798	
software, algorithm	CytExpert	Beckman Coulter	RRID: SCR_017217	
software, algorithm	ImageJ	National Institutes of Health	RRID: SCR_003070	

Figure 1

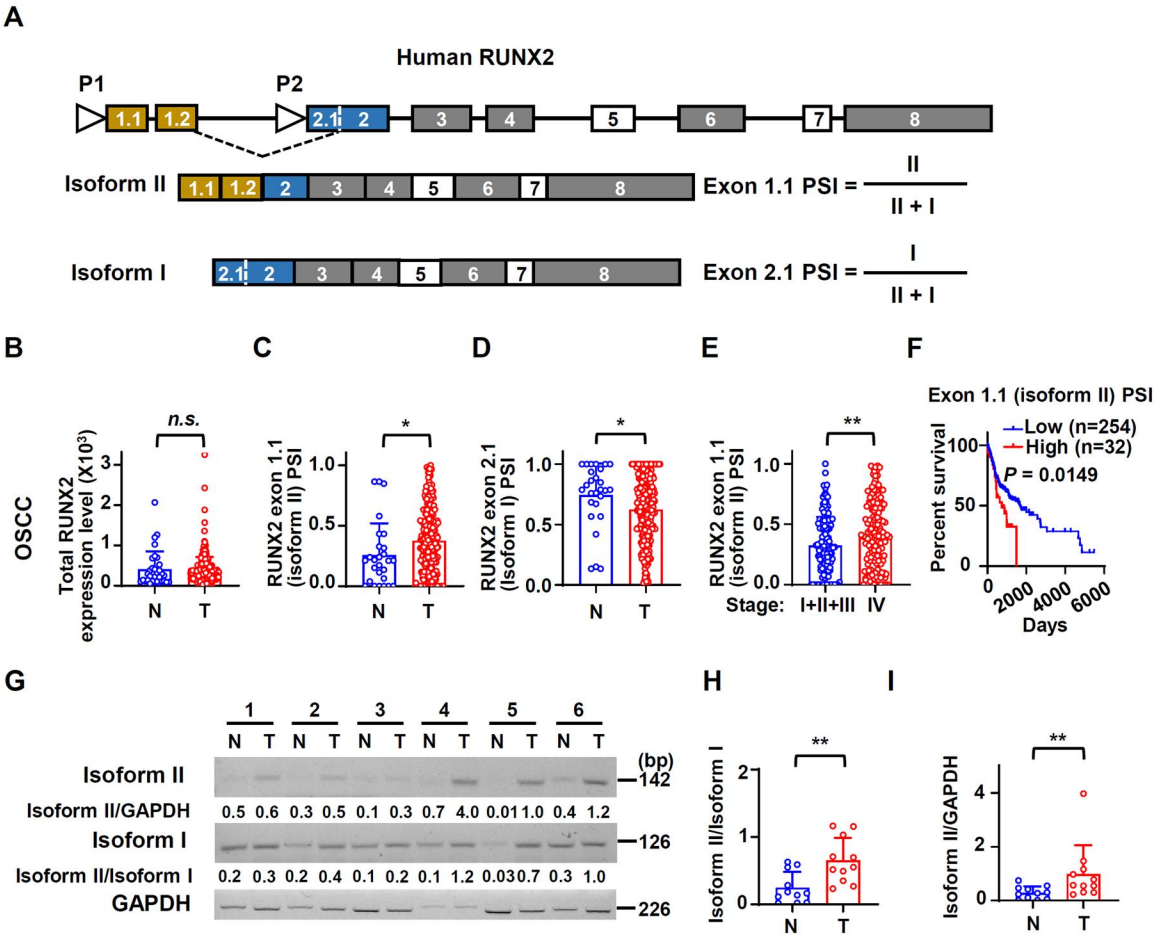
A
Human RUNX2
P1
P2
1.1
1.2
2.1
2
3
4
5
6
7
8
Isoform II
Exon 1.1 PSI = II / II + I
Isoform I
Exon 2.1 PSI = I / II + I
B
OSCC
Total RUNX2 expression level (X10³)
n.s.
N
T
C
RUNX2 exon 1.1 (isoform II) PSI
*
D
RUNX2 exon 2.1 (Isoform I) PSI
*
E
RUNX2 exon 1.1 (isoform II) PSI
**
Stage: I+II+III IV
F
Exon 1.1 (isoform II) PSI
Low (n=254)
High (n=32)
P = 0.0149
Percent survival
Days
G
Isoform II
Isoform II/GAPDH
0.5 0.6 0.3 0.5 0.1 0.3 0.7 4.0 0.01 1.0 0.4 1.2
Isoform I
Isoform II/Isoform I
0.2 0.3 0.2 0.4 0.1 0.2 0.1 1.2 0.03 0.7 0.3 1.0
GAPDH
(bp)
142
126
226
H
Isoform II/Isoform I
**
I
Isoform II/GAPDH
**

Figure 2

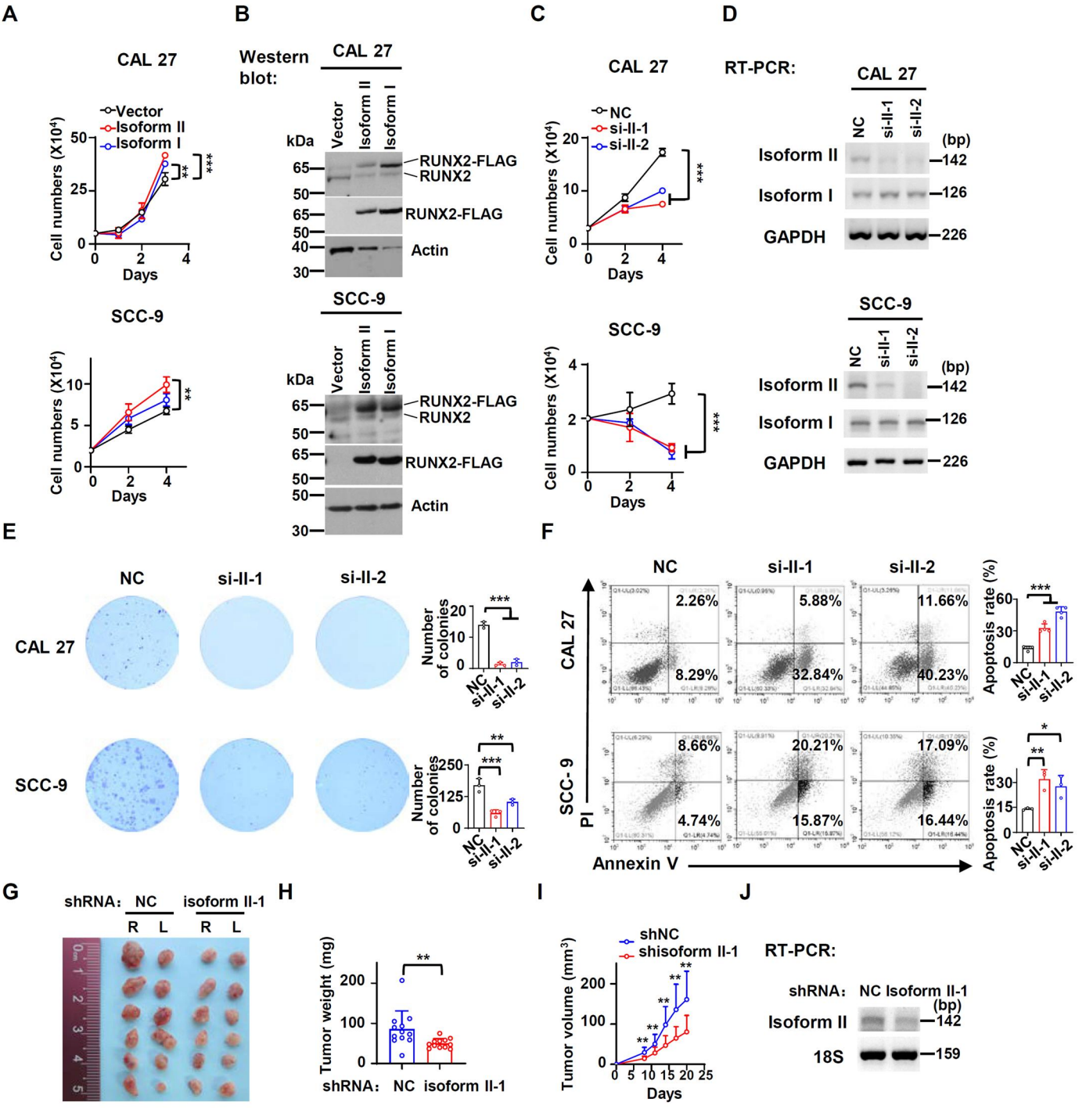
A
CAL 27
Vector
Isoform II
Isoform I
Cell numbers (X10⁴)
Days
SCC-9
B
Western blot:
CAL 27
Vector
Isoform II
Isoform I
kDa
RUNX2-FLAG
RUNX2
Actin
SCC-9
C
CAL 27
NC
si-II-1
si-II-2
Cell numbers (X10⁴)
Days
SCC-9
D
RT-PCR:
CAL 27
NC
si-II-1
si-II-2
(bp)
Isoform II
Isoform I
GAPDH
142
126
226
SCC-9
E
NC
si-II-1
si-II-2
CAL 27
SCC-9
Number of colonies
F
NC
si-II-1
si-II-2
CAL 27
SCC- 9
PI
Annexin V
2.26%
8.29%
5.88%
32.84%
11.66%
40.23%
8.66%
4.74%
20.21%
15.87%
17.09%
16.44%
Apoptosis rate (%)
G
shRNA: NC
isoform II-1
R
L
H
Tumor weight (mg)
shRNA: NC
isoform II-1
I
shNC
shisoform II-1
Tumor volume (mm³)
Days
J
RT-PCR:
shRNA: NC Isoform II-1
(bp)
Isoform II
18S
142
159

Figure 3

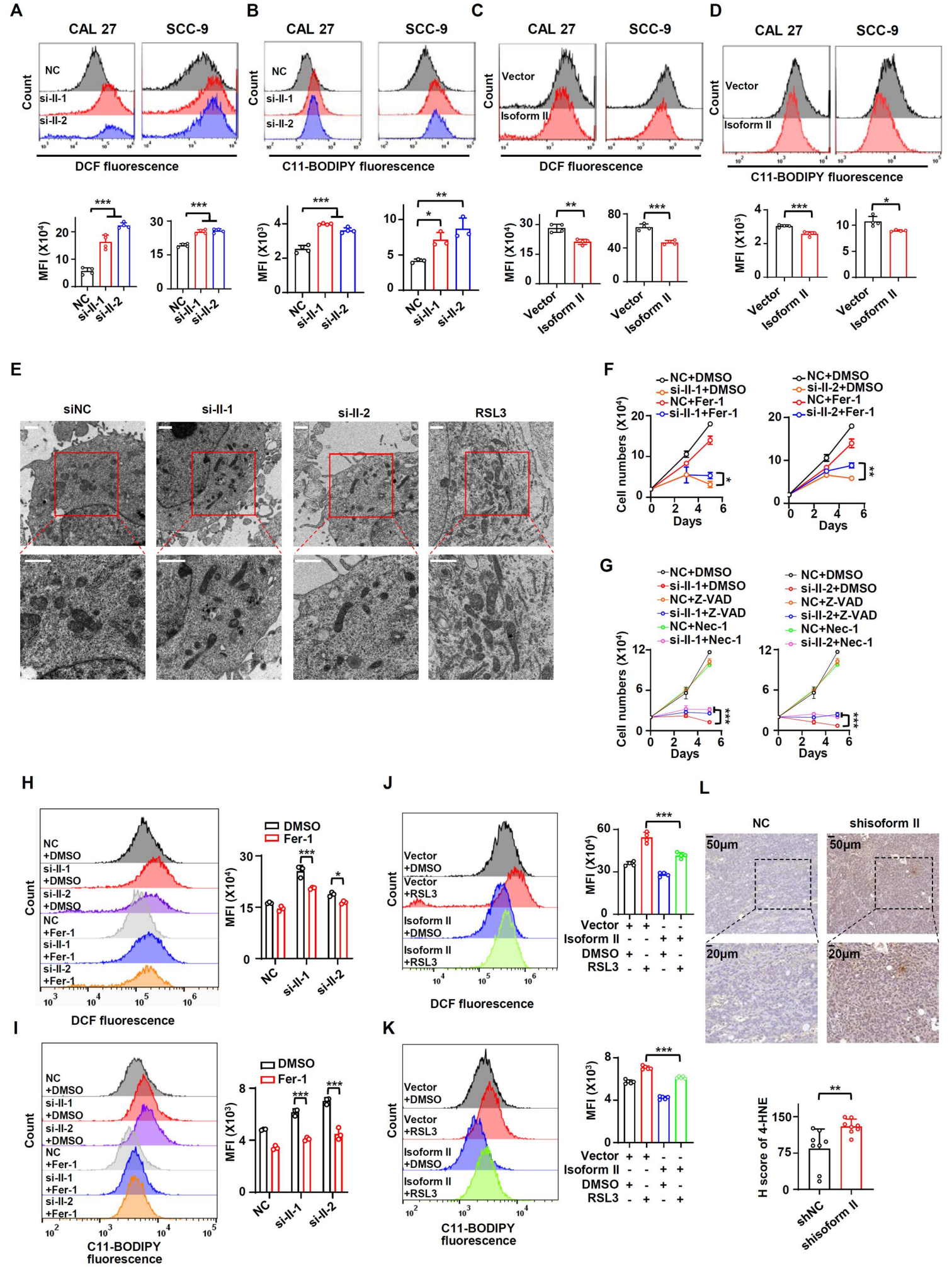
A
CAL 27
SCC-9
NC
si-II-1
si-II-2
Count
DCF fluorescence
MFI (X10⁴)
B
C11-BODIPY fluorescence
MFI (X10³)
C
Vector
Isoform II
D
E
siNC
si-II-1
si-II-2
RSL3
F
NC+DMSO
si-II-1+DMSO
NC+Fer-1
si-II-1+Fer-1
si-II-2+DMSO
si-II-2+Fer-1
Cell numbers (X10⁴)
Days
G
NC+Z-VAD
si-II-1+Z-VAD
NC+Nec-1
si-II-1+Nec-1
si-II-2+Z-VAD
si-II-2+Nec-1
H
DMSO
Fer-1
I
J
Vector +DMSO
Vector +RSL3
Isoform II +DMSO
Isoform II +RSL3
K
L
NC
shisoform II
50μm
20μm
H score of 4-HNE
shNC
shisoform II

Figure 4

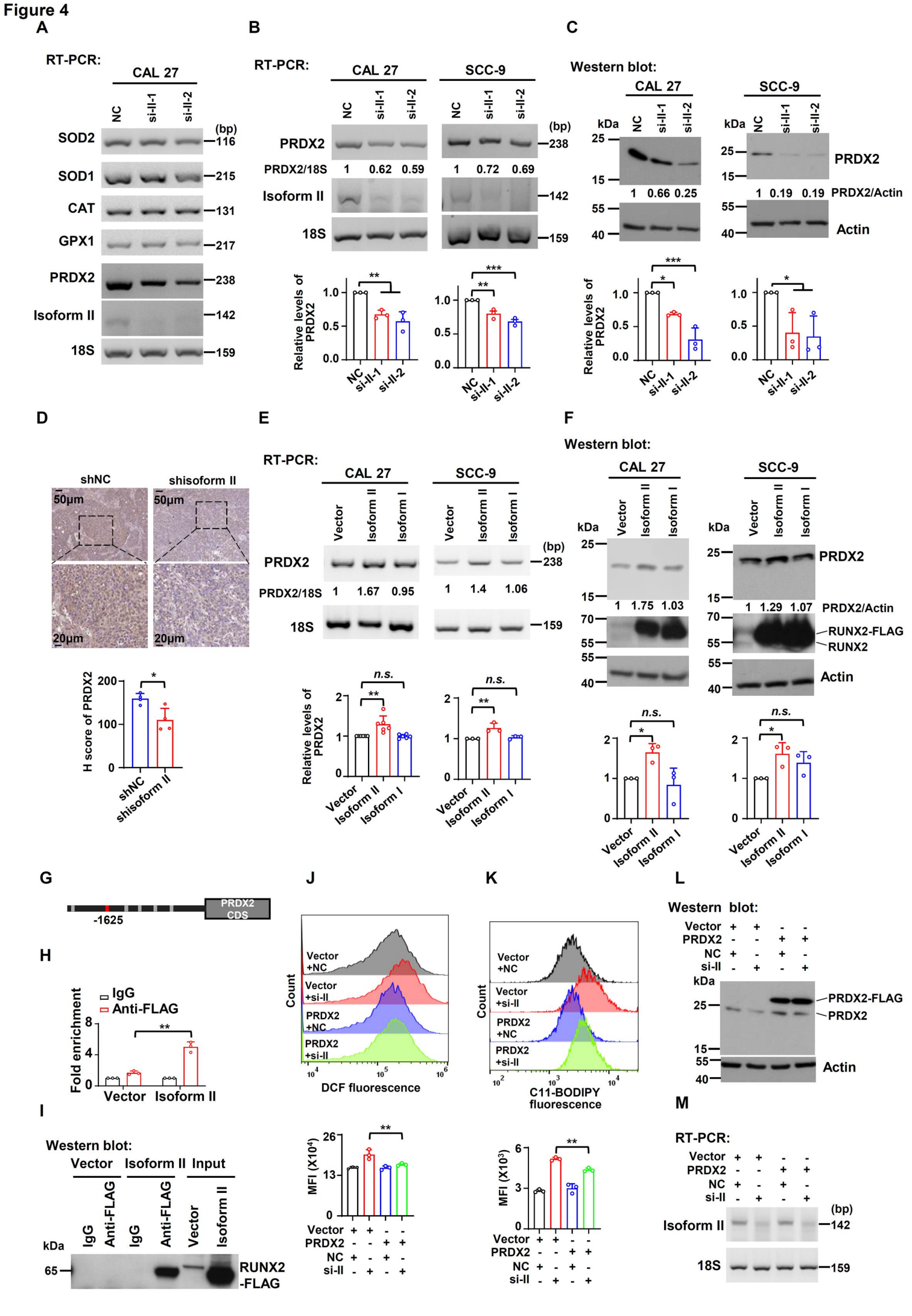
A
RT-PCR:
CAL 27
NC
si-II-1
si-II-2
(bp)
SOD2
116
SOD1
215
CAT
131
GPX1
217
PRDX2
238
Isoform II
142
18S
159
B
RT-PCR:
CAL 27
SCC-9
PRDX2
PRDX2/18S
1 0.62 0.59
1 0.72 0.69
Isoform II
18S
Relative levels of PRDX2
C
Western blot:
kDa
25
15
55
40
1 0.66 0.25
1 0.19 0.19
PRDX2/Actin
Actin
D
shNC
shisoform II
50μm
20μm
H score of PRDX2
200
100
0
E
RT-PCR:
Vector
Isoform II
Isoform I
PRDX2/18S
1 1.67 0.95
1 1.4 1.06
n.s.
F
Western blot:
70
1 1.75 1.03
1 1.29 1.07
RUNX2-FLAG
RUNX2
G
PRDX2 CDS
-1625
H
IgG
Anti-FLAG
Fold enrichment
Vector
Isoform II
I
Western blot:
Vector
Isoform II
Input
IgG
Anti-FLAG
RUNX2 -FLAG
J
Count
Vector +NC
Vector +si-II
PRDX2 +NC
PRDX2 +si-II
DCF fluorescence
MFI (X10⁴)
K
C11-BODIPY fluorescence
MFI (X10³)
L
Western blot:
PRDX2-FLAG
PRDX2
M
RT-PCR:
Isoform II
18S

Figure 5

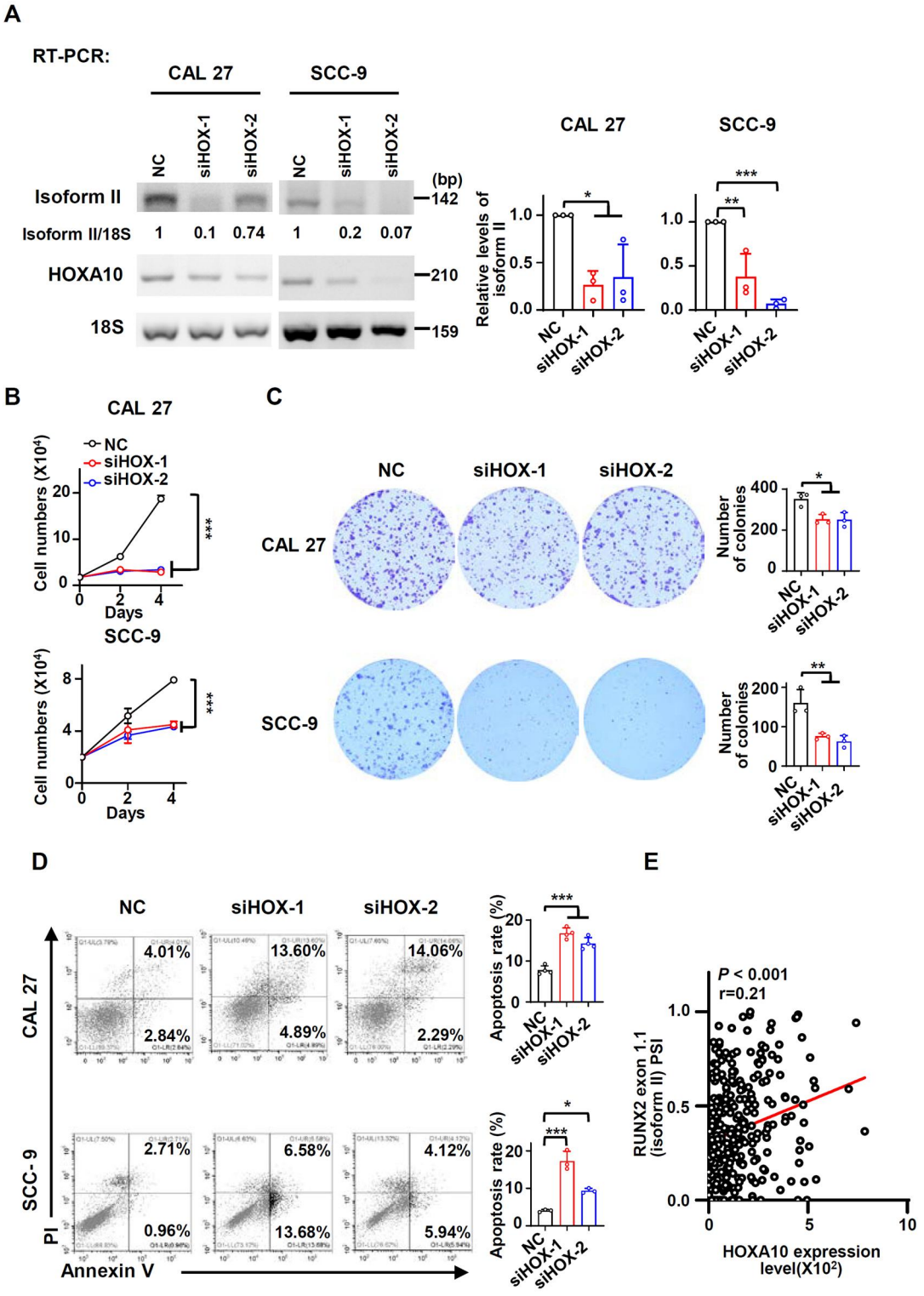
A
RT-PCR:
CAL 27
SCC-9
NC
siHOX-1
siHOX-2
(bp)
Isoform II
142
Isoform II/18S
1
0.1
0.74
1
0.2
0.07
HOXA10
210
18S
159
Relative levels of isoform II
B
Cell numbers (X10⁴)
Days
C
Number of colonies
D
Apoptosis rate (%)
4.01%
2.84%
13.60%
4.89%
14.06%
2.29%
2.71%
0.96%
6.58%
13.68%
4.12%
5.94%
PI
Annexin V
E
P < 0.001
r=0.21
RUNX2 exon 1.1 (isoform II) PSI
HOXA10 expression level(X10²)

Figure 6

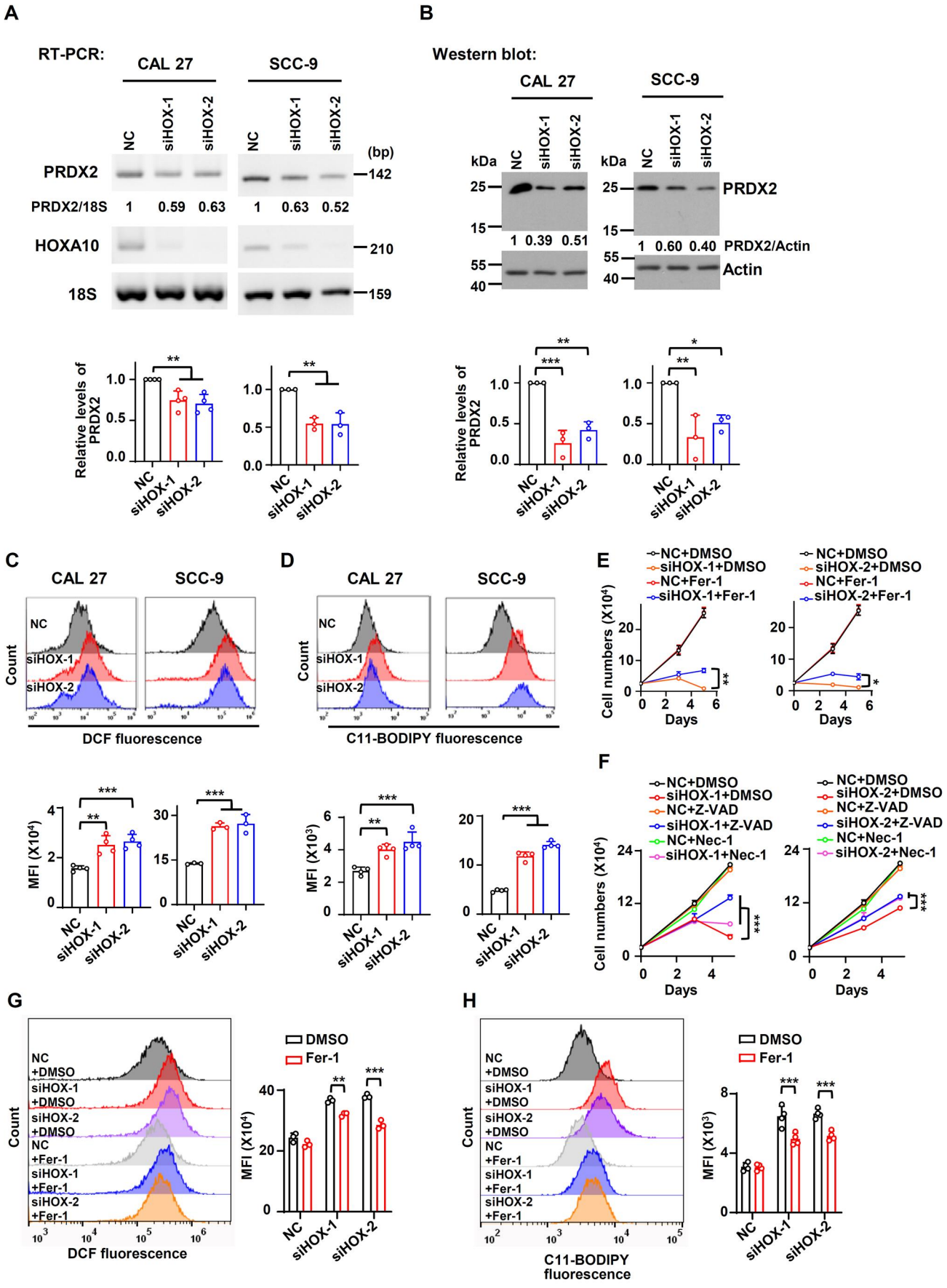
A
RT-PCR:
CAL 27
SCC-9
NC
siHOX-1
siHOX-2
(bp)
PRDX2
142
PRDX2/18S
1
0.59
0.63
1
0.63
0.52
HOXA10
210
18S
159
Relative levels of PRDX2
B
Western blot:
kDa
25
15
PRDX2
1
0.39
0.51
1
0.60
0.40
PRDX2/Actin
55
40
Actin
C
Count
DCF fluorescence
MFI (X10⁴)
D
C11-BODIPY fluorescence
MFI (X10³)
E
NC+DMSO
siHOX-1+DMSO
siHOX-2+DMSO
NC+Fer-1
siHOX-1+Fer-1
siHOX-2+Fer-1
Cell numbers (X10⁴)
Days
F
NC+Z-VAD
siHOX-1+Z-VAD
siHOX-2+Z-VAD
NC+Nec-1
siHOX-1+Nec-1
siHOX-2+Nec-1
G
NC +DMSO
siHOX-1 +DMSO
siHOX-2 +DMSO
NC +Fer-1
siHOX-1 +Fer-1
siHOX-2 +Fer-1
DMSO
Fer-1
H

Figure 7

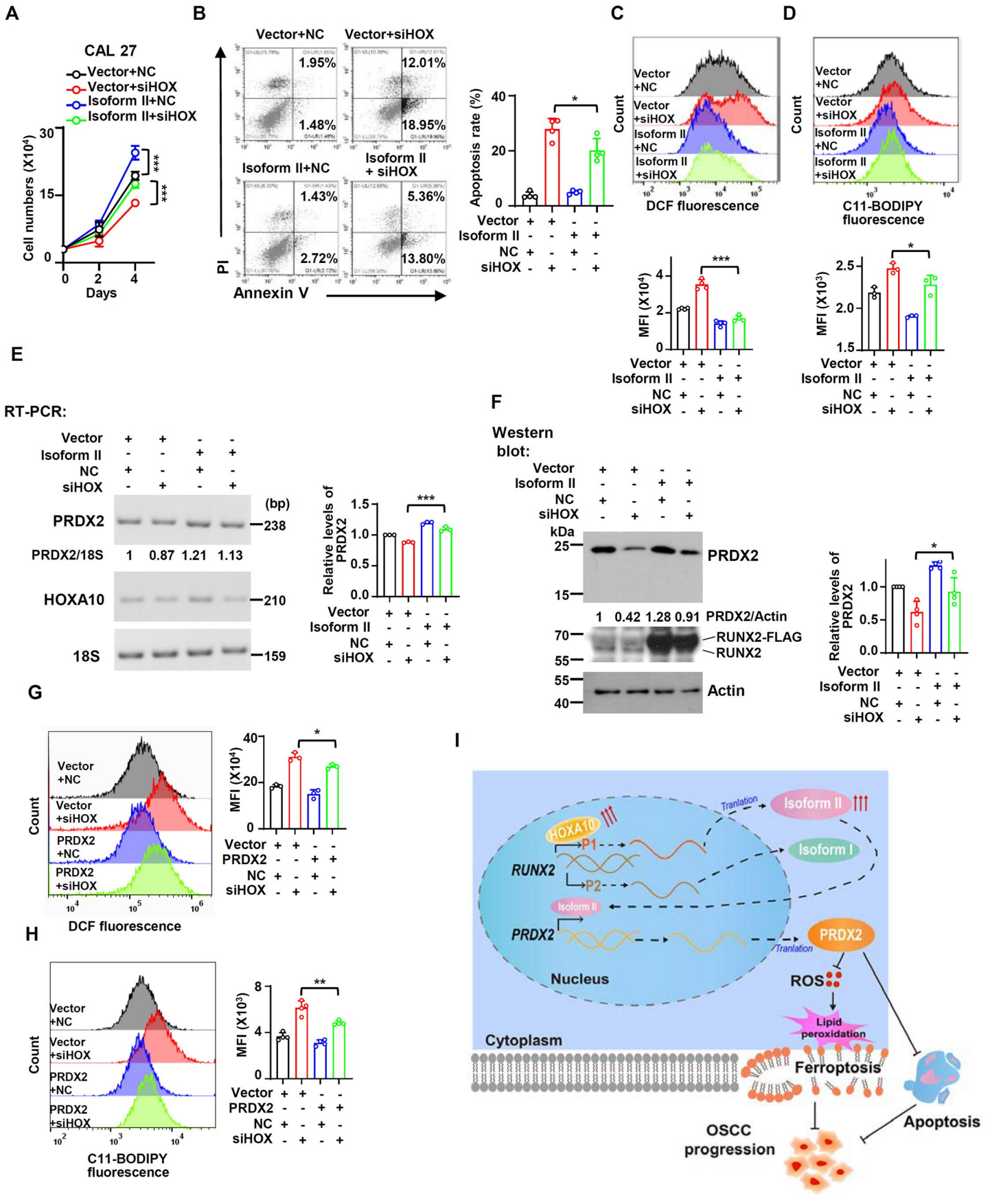
A
CAL 27
Vector+NC
Vector+siHOX
Isoform II+NC
Isoform II+siHOX
Cell numbers (X10⁴)
Days
B
Vector+NC
Vector+siHOX
Isoform II+NC
Isoform II + siHOX
PI
Annexin V
Apoptosis rate (%)
C
Count
DCF fluorescence
MFI (X10⁴)
D
C11-BODIPY fluorescence
MFI (X10³)
E
RT-PCR:
PRDX2
HOXA10
18S
PRDX2/18S 1 0.87 1.21 1.13
Relative levels of PRDX2
F
Western blot:
kDa
PRDX2
1 0.42 1.28 0.91 PRDX2/Actin
RUNX2-FLAG
RUNX2
Actin
G
DCF fluorescence
H
C11-BODIPY fluorescence
I
Tranlation
Isoform II
Isoform I
HOXA10
P1
P2
RUNX2
PRDX2
Nucleus
ROS
Lipid peroxidation
Cytoplasm
Ferroptosis
Apoptosis
OSCC progression

Figure 1-figure supplement 1

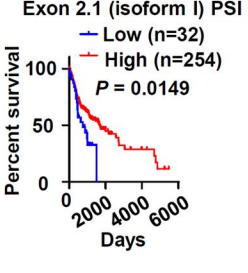

Figure 1-figure supplement 2

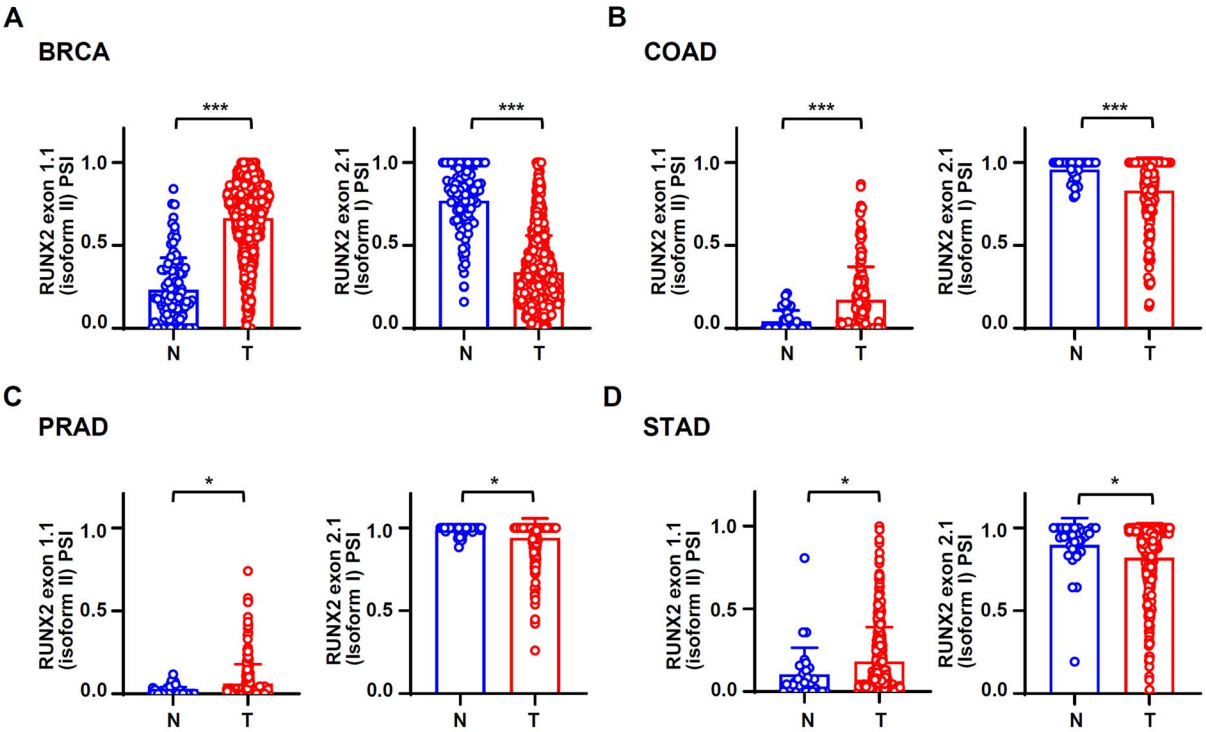

Figure 2-figure supplement 1

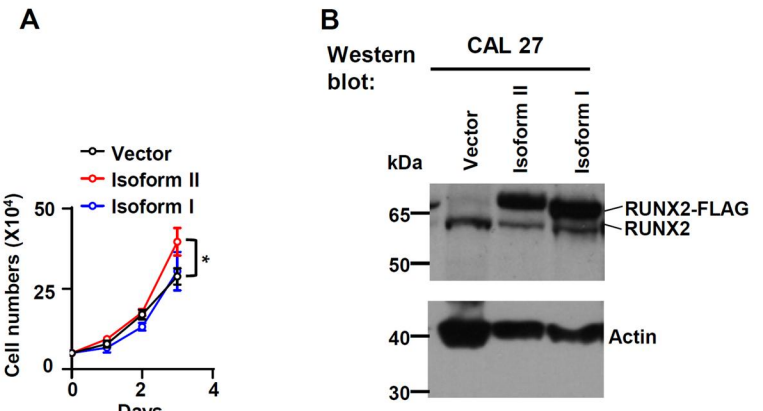

Figure 2-figure supplement 2

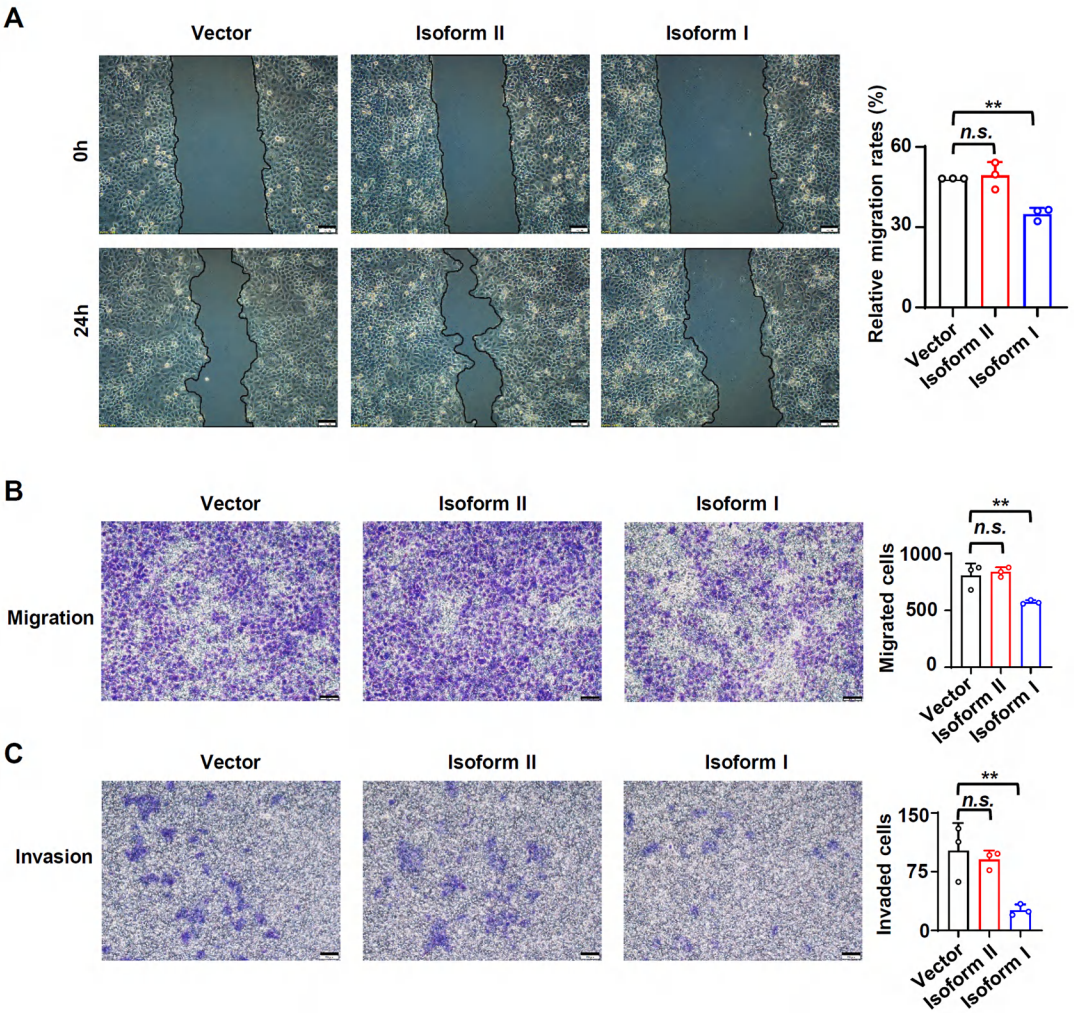

Figure 2-figure supplement 3

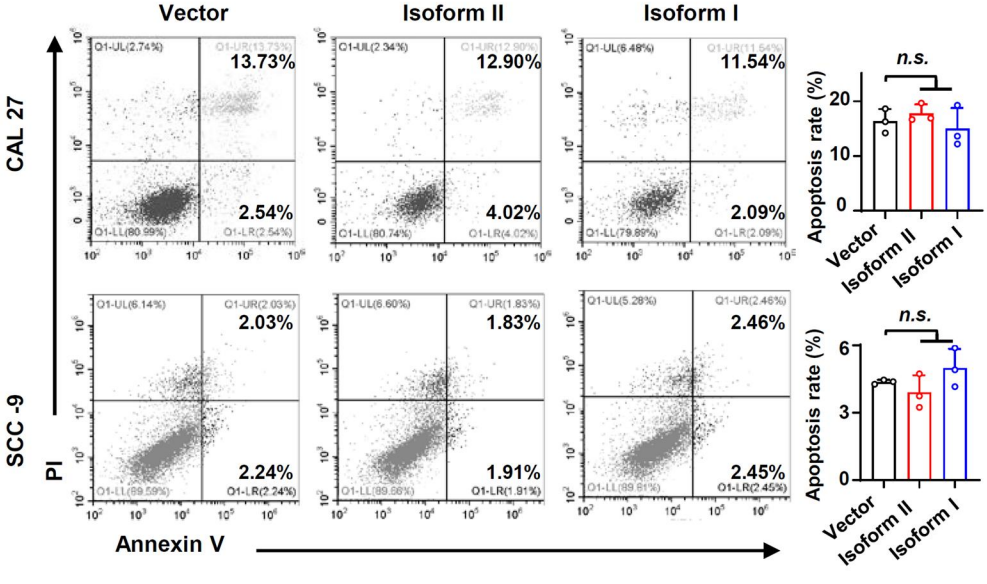

Figure 2-figure supplement 4

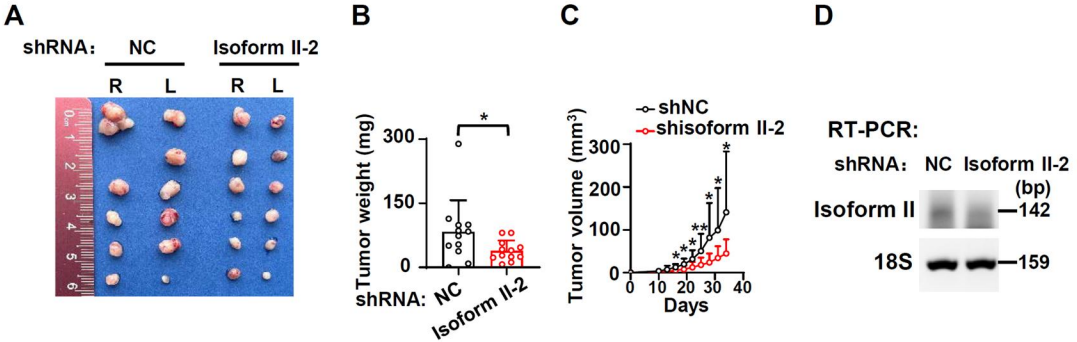

Figure 3-figure supplement 1

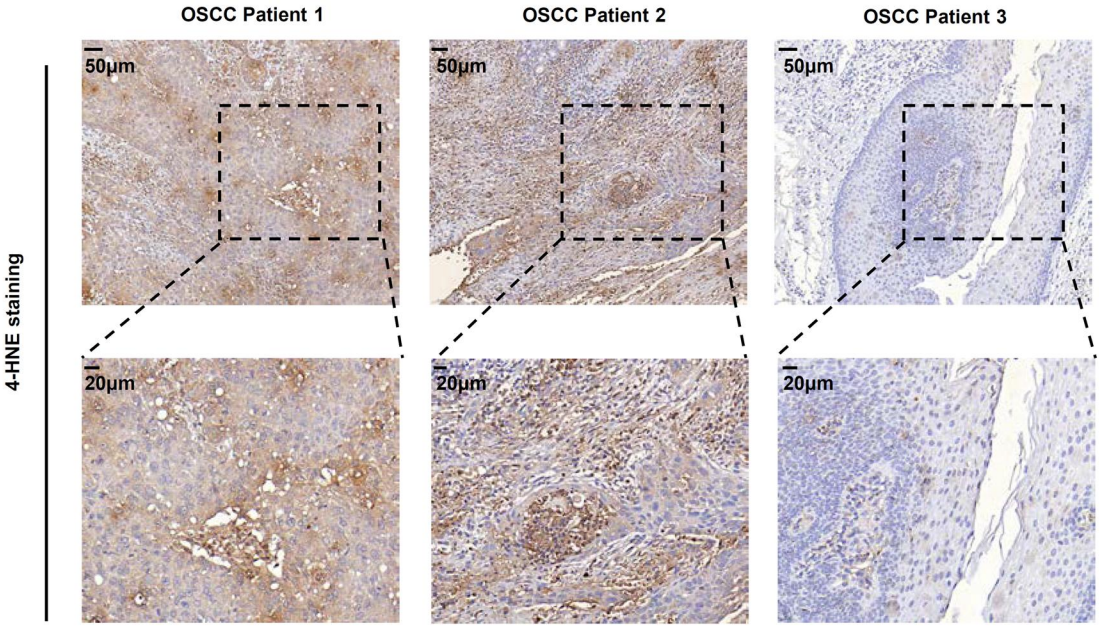

Figure 3-figure supplement 2

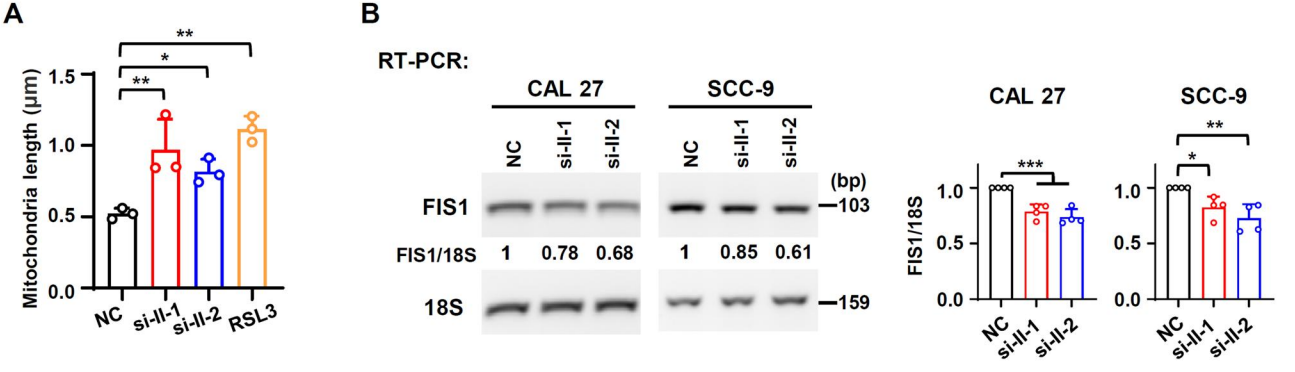

Figure 3-figure supplement 3

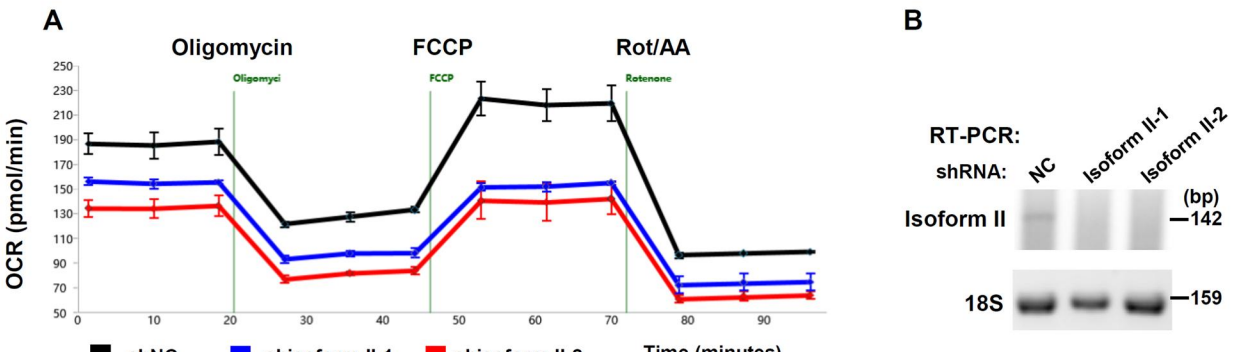

Figure 3-figure supplement 4

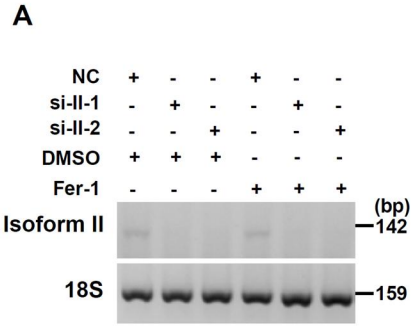

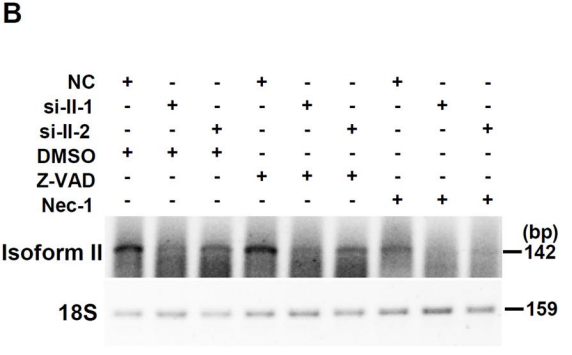

Figure 3-figure supplement 5

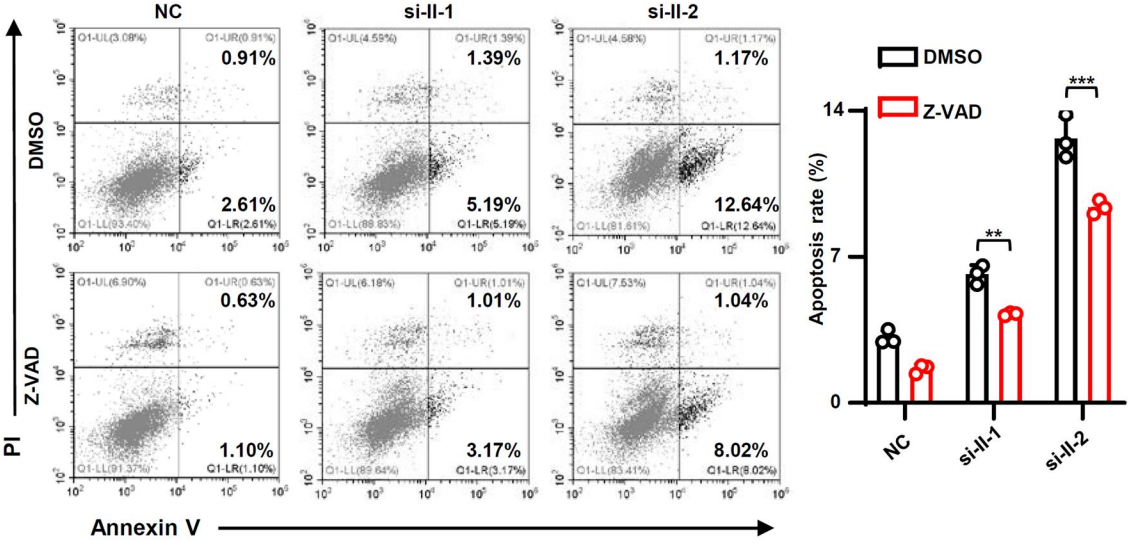

Figure 3-figure supplement 6

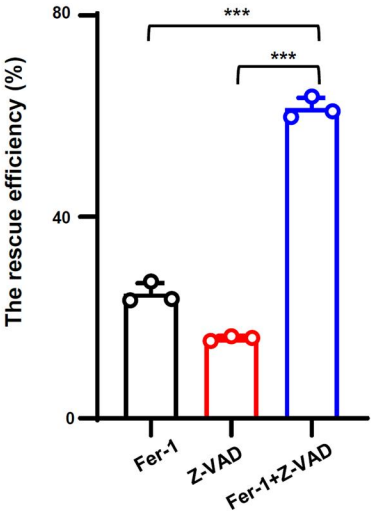

Figure 3-figure supplement 7

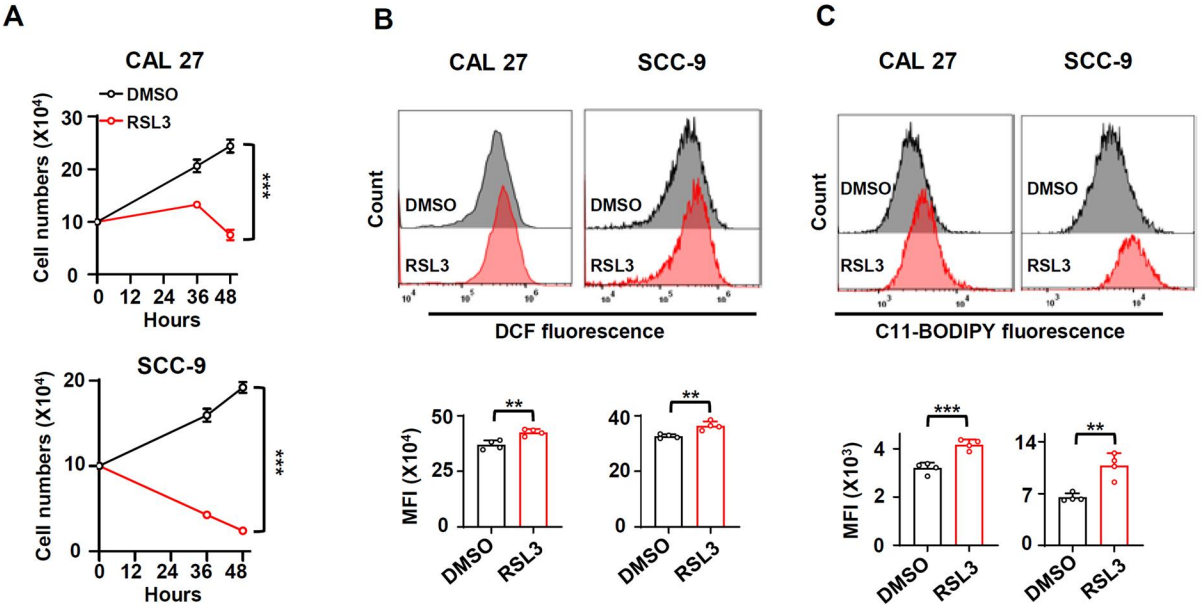

Figure 3-figure supplement 8

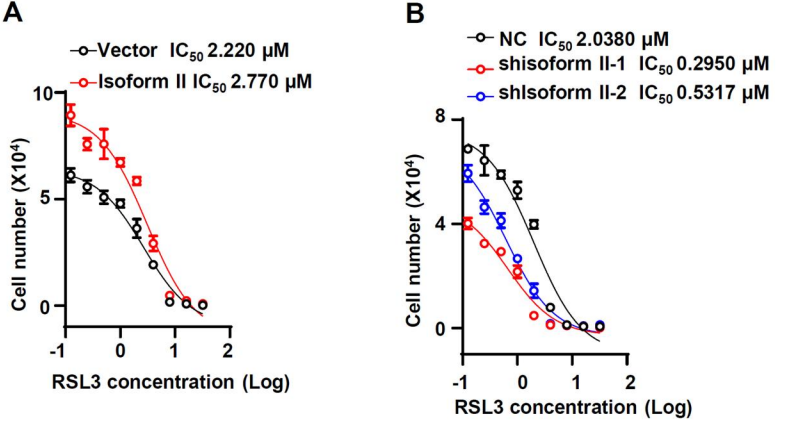

Figure 4-figure supplement 1

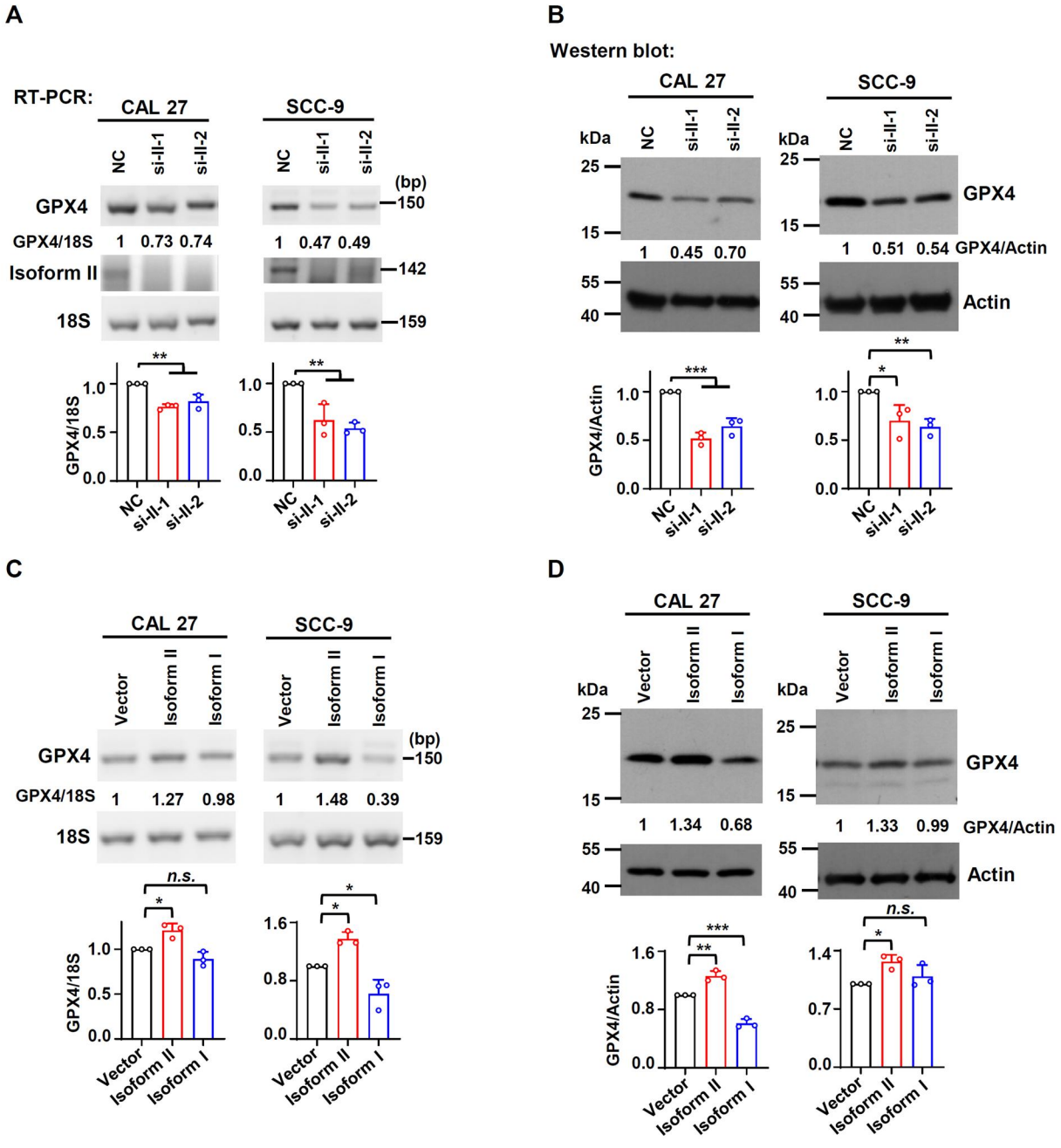

Figure 4-figure supplement 2

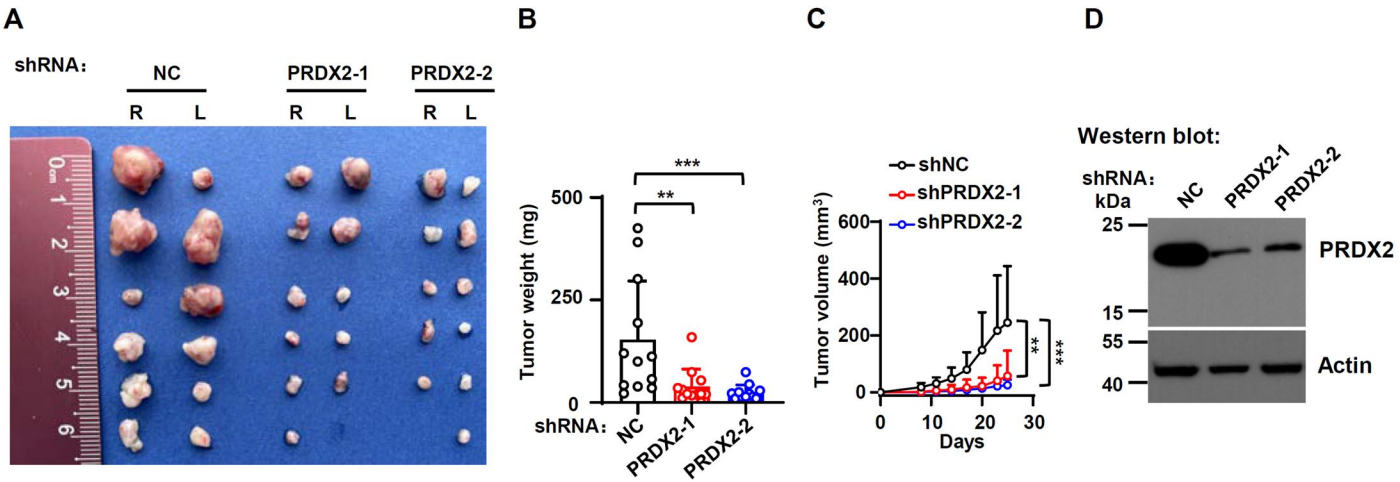

Figure 4-figure supplement 3

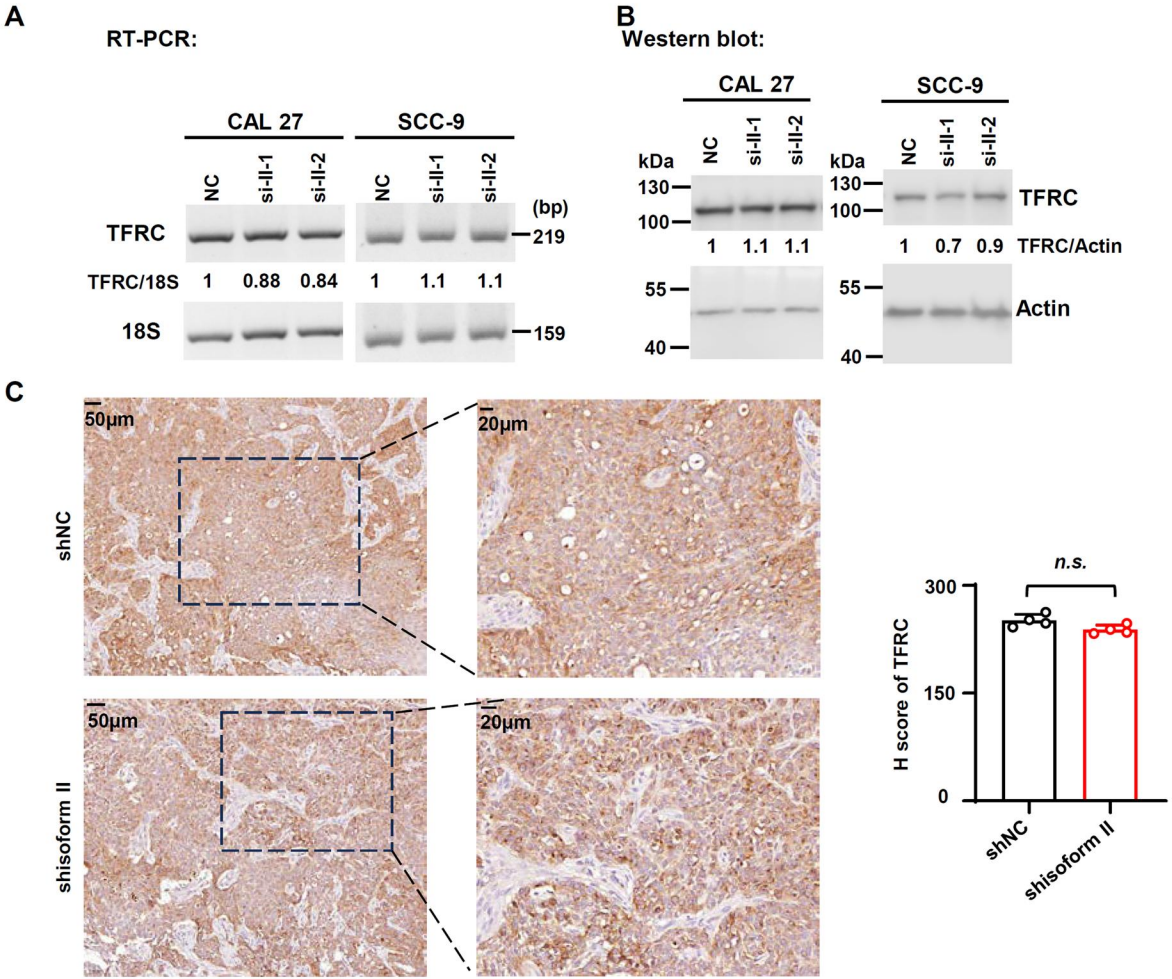

Figure 4-figure supplement 4

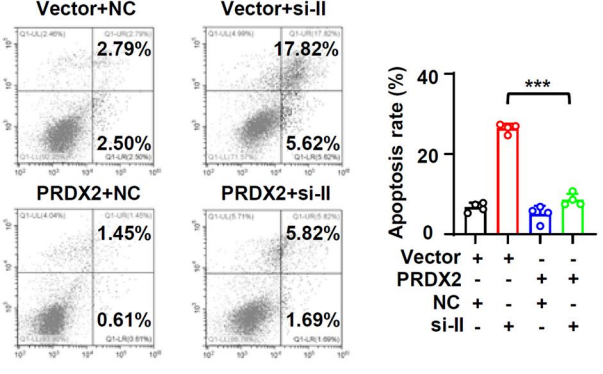

Figure 5-figure supplement 1

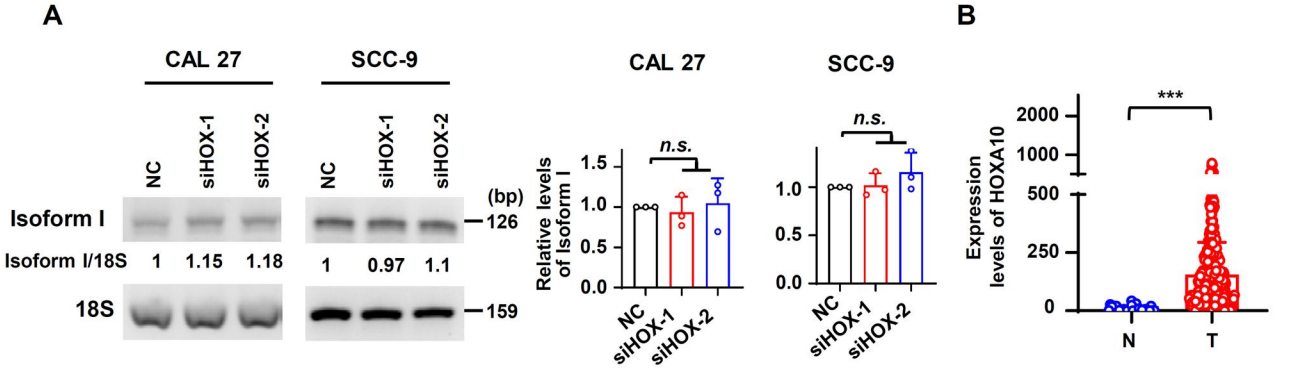

Figure 5-figure supplement 2

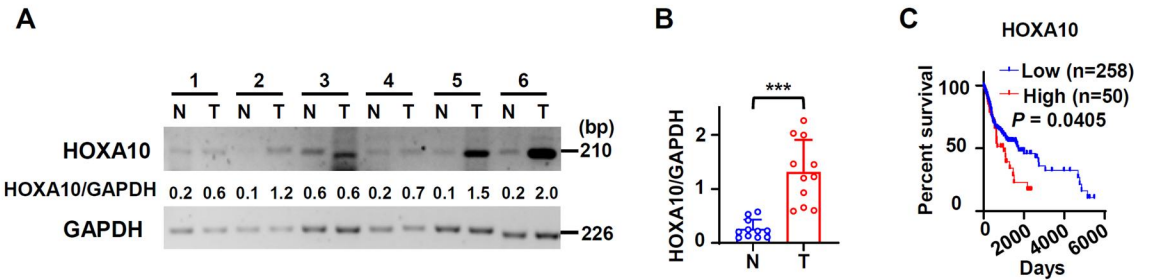

Figure 6-figure supplement 1

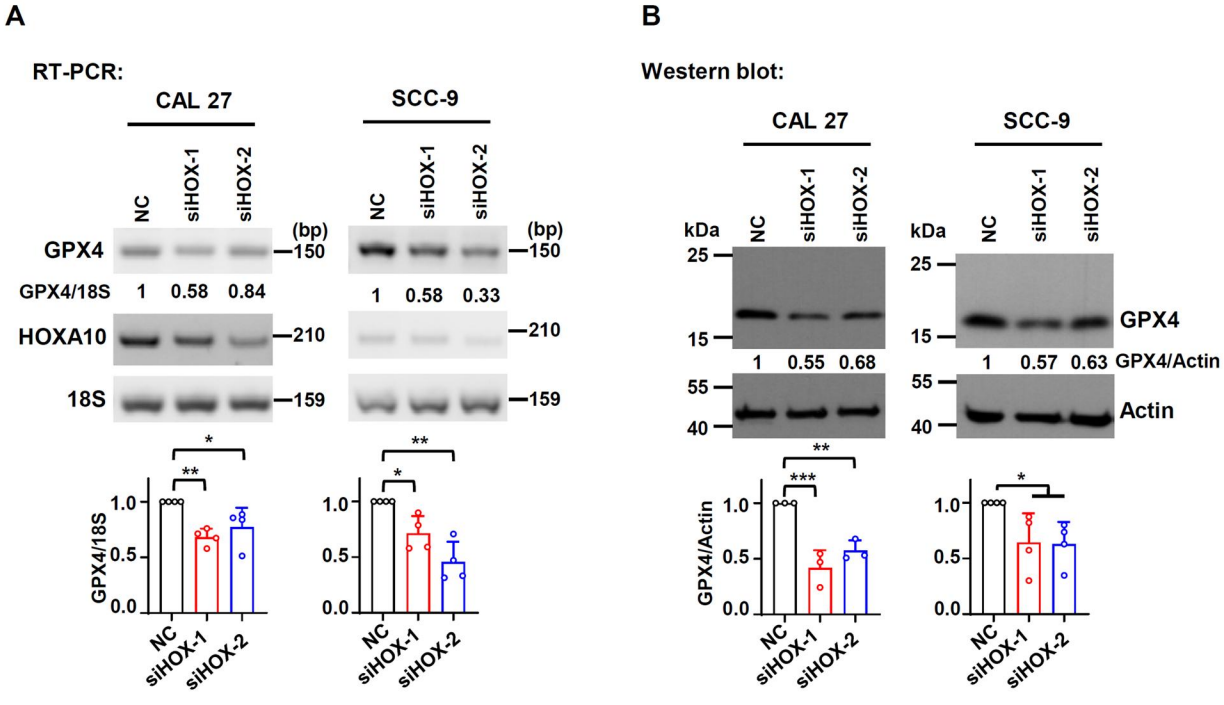

Figure 6-figure supplement 2

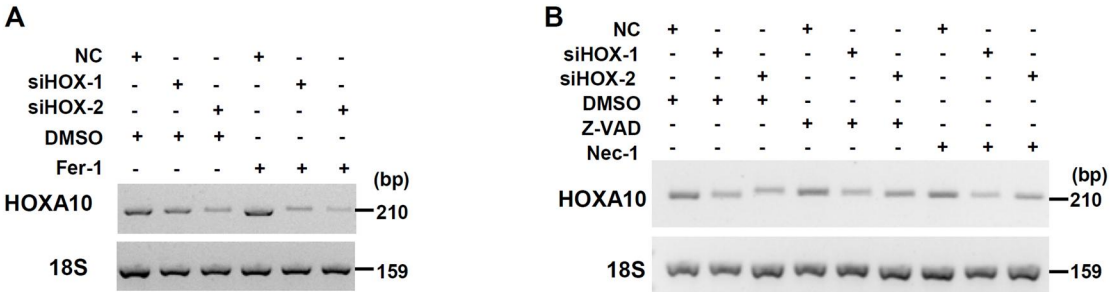

Figure 6-figure supplement 3

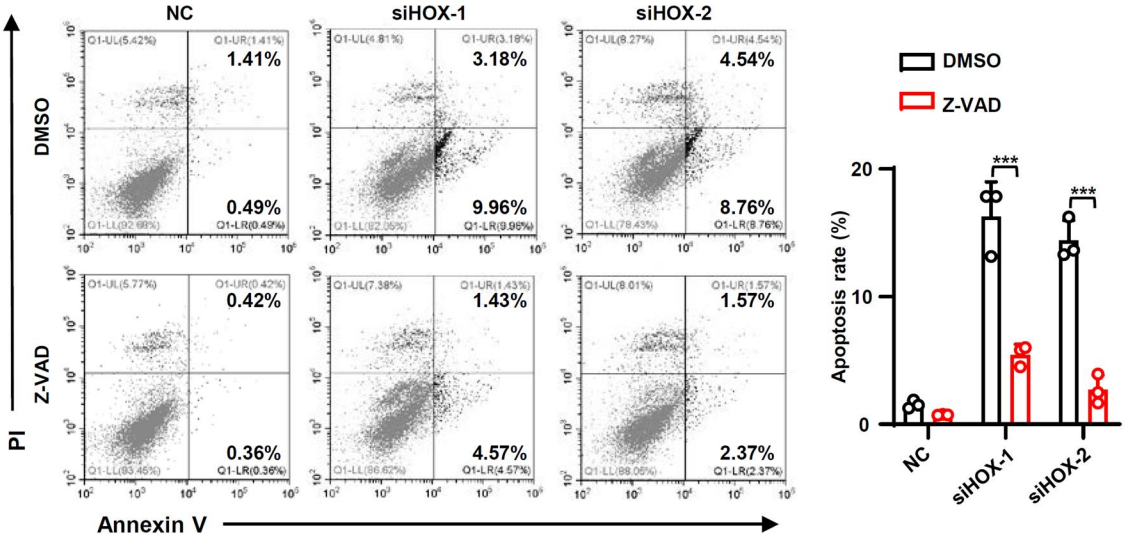

Figure 6-figure supplement 4

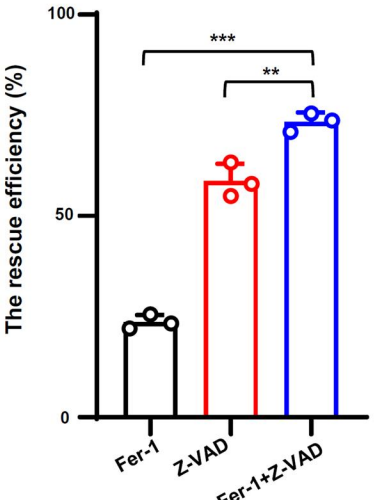

Figure 7-figure supplement 1

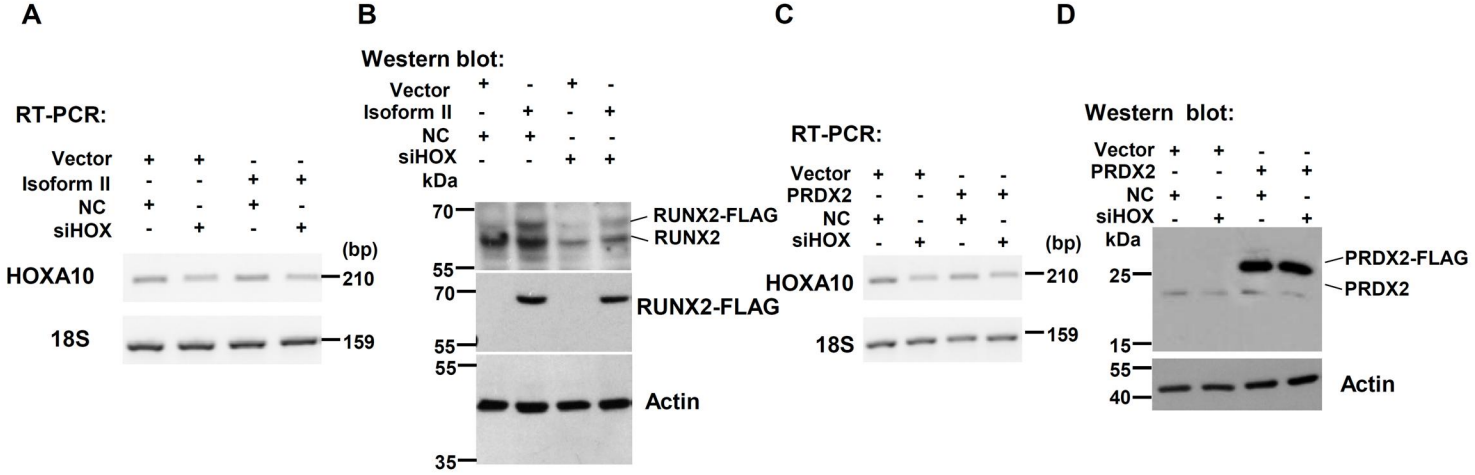

Figure 7-figure supplement 2

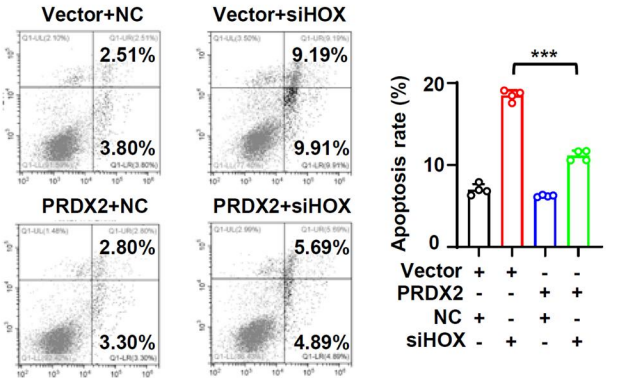

The clinical characteristics of OSCC patients

Characteristics	Number of Cases (%)
Age (Y)	
<55	4 (36.4%)
≥55	7 (63.6%)
Gender	
Male	9 (81.8%)
Female	2 (18.2%)

Primer sequences for RT-PCR

Gene name	Sequence
RUNX2 isoform II	F: 5’ GCACAGTGACACCATGTCAGC 3’ R: 5’ TGCTGTTGCTGCTGCTGTTG 3’
RUNX2 isoform I	F: 5’ TGTGATGCGTATTCCCGTAGATC 3’ R: 5’ TGCTGTTGCTGCTGCTGTTG 3’
PRDX2	F: 5’ CCAGACGCTTGTCTGAGGAT 3’ R: 5’ ACGTTGGGCTTAATCGTGTC 3’
SOD1	F: 5’ AAGGCCGTGTGCGTGCTGAA 3’ R: 5’ GGCCCACCGTGTTTTCTGGA 3’
SOD2	F: 5’ GGAAGCCATCAAACGTGACTT 3’ R: 5’ CCCGTTCCTTATTGAAACCAAGC 3’
CAT	F: 5’ CCAGAAGAAAGCGGTCAAGAA 3’ R: 5’ GAGATCCGGACTGCACAAAG 3’
GPX1	F: 5’ TCGGTGTATGCCTTCTCGG 3’ R: 5’ CGTTCTCCTGATGCCCAAA 3’
HOXA10	F: 5’ AGAGATTAGCCGCAGCGTCC 3’ R: 5’ TTCCTGGGCAGAGCCTGAAG 3’
GAPDH	F: 5’ GAAGGTGAAGGTCGGAGTC 3’ R: 5’ GAAGATGGTGATGGGATTTC 3’
Human 18S rRNA	F: 5’ GGATGCGTGCATTTATCAGA 3’ R: 5’ GTTGATAGGGCAGACGTTCG 3’
TFRC	F: 5' ACCATTGTCATATACCCGGTTCA 3' R: 5' CAATAGCCCAAGTAGCCAATCAT 3'
FIS1	F: 5' CGGAGCAAGTACAATGATGAC 3' R: 5' CCAGGTAGAAGACGTAATCCC 3'